# WATER-COLUMN INERTIAL AND SUB-INERTIAL OCEANIC RESPONSE TO HURRICANE ISAAC IN THE DEEPWATER GULF OF MEXICO

A Thesis

by

LAURA JEAN SPENCER

Submitted to the Office of Graduate and Professional Studies of
Texas A&M University
in partial fulfillment of the requirements for the degree of

MASTER OF SCIENCE

| | |
|---|---|
| Chair of Committee, | Steven DiMarco |
| Committee Members, | David Brooks |
| | Kenneth Bowman |
| Head of Department, | Debbie Thomas |

December 2014

Major Subject: Oceanography

# ABSTRACT

Tropical Storm Isaac entered the Gulf of Mexico on 27 August 2012 and strengthened to become a Category 1 hurricane shortly before making landfall in southern Louisiana. Hurricane Isaac approached Southwest Pass near the mouth of the Mississippi River on August 29, 2012 at 00:00 UTC. The center of the storm then moved westward before making landfall eight hours later at Port Fourchon, LA. On August 28, 2012 at approximately 18:00 UTC, Hurricane Isaac passed directly over the center of a mooring array in a northwesterly trajectory. As part of the Gulf Integrated Spill Research Program, six deepwater moorings featuring upward-looking 75 kHz Acoustic Doppler Current Profilers were deployed in water depths between 836 m and 1690 m in the Mississippi Fan region of the northern Gulf of Mexico in July 2012. Each of the six moorings featured 3 Aanderaa RCM current meters. One current meter was located near the bottom, the next positioned approximately 180 m shallower, then the last positioned an additional 200 m shallower. One mooring featured four InterOcean S4A current meters positioned 100 m apart between 790 m and 1090 m. Maximum current speeds of 41.3 cm/s at 100 m, 35.5 cm/s at 300 m, and 32.7 cm/s at 500 m depth were observed during the passage of the Hurricane Isaac. Maximum bottom current speeds measured from Aanderaa RCMs ranged between 16.1 cm/s at 1645 m depth and 34.0 cm/s at 1020 m depth. Inertial band oscillations (1/2-2 days) are seen to 800 m depths, with energy propagation speeds on the order of 30 m/day vertically and 5.7 km/day horizontally. A

blue shift in the effective frequency to 1.11*f* is observed in the near-inertial band in the wake of Hurricane Isaac. Wavelet analyses of the time-series records indicate two sub-inertial oscillations (2-5 days and 5-12 days) initiated throughout the water-column at the time of the storms closest approach that persist for approximately one week. Each sub-inertial band response was fundamentally different from the near-inertial response to Hurricane Isaac and showed a strong barotropic response.

ACKNOWLEDGEMENTS

I would like to thank my committee chair, Dr. Steven DiMarco, and my committee members, Dr. David Brooks, and Dr. Kenneth Bowman, for their guidance and support throughout the course of this research.

Thanks also goes to my friends and colleagues and the wonderful and dedicated faculty and staff for making my graduate and undergraduate career at Texas A&M such a wonderful time in life. I also want to extend my gratitude to the Gulf Integrated Spill Research Consortium and the Gulf of Mexico Research Initiative that provided the funding and invaluable research cruise experience. I would also like to thank the captain and crew of the R.V. Pelican for their help with the deployment and recovery of the mooring systems used in this study. Thanks also goes Dr. Robert Leben for the use of his satellite altimetry products used in this study as well as Drs. Christopher Torrence and Gilbert Compo for the use of their Wavelet package which can be found at http://paos.colorado.edu/research/wavelets.

A special thanks goes to my high school science teachers, Mr. Eulin Cain and Mr. Stacey Burkett, for instilling in me a deep love of science and successfully preparing me for my exciting journey at Texas A&M. Without their guidance and support I would not be where I am today.

Finally, thanks to my mother and father for their encouragement, support and love, and to my wonderful husband for his patience and love.

TABLE OF CONTENTS

Page

LIST OF FIGURES

Page

LIST OF TABLES

Page

# 1. INTRODUCTION

Tropical Storm Isaac entered the Gulf of Mexico in late August 2012 as a tropical storm and strengthened to become a Category 1 hurricane. Hurricane Isaac passed directly over a deepwater current-meter mooring array deployed along the continental slope in the Mississippi Fan region of the northern Gulf of Mexico hours before making landfall in southern Louisiana on August 29, 2012. Acoustic Doppler Current Profilers and current meters deployed in the mooring array observed the full water-column oceanic response to the hurricane (Figure 1).

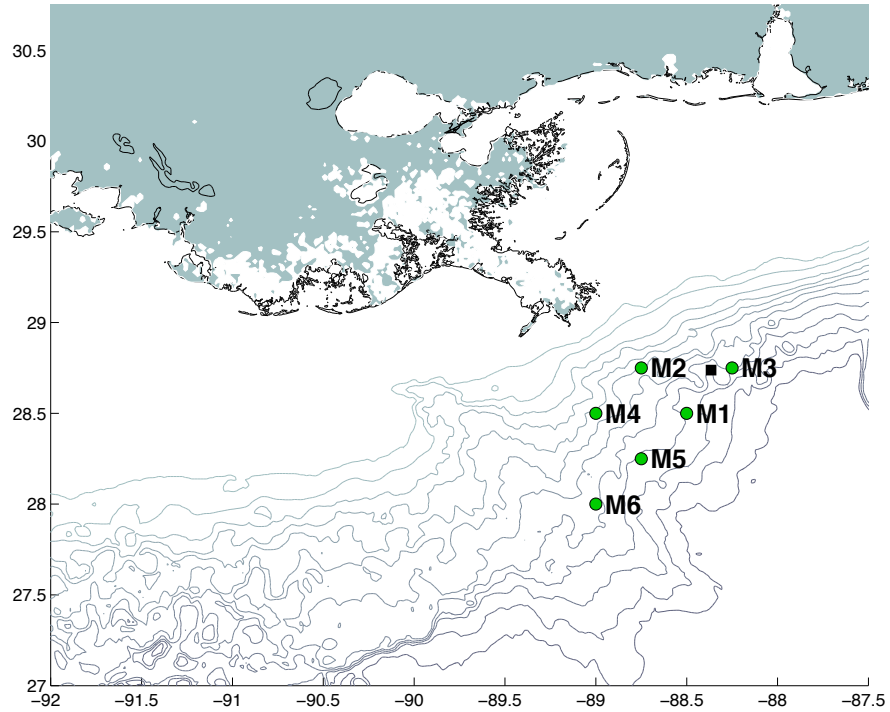


Figure 1. GISR Mooring Array. A basemap of mooring locations in Northern Gulf of Mexico (green circles) is presented. Bathymetry lines are shown every 200m beginning at 200m and ending at 2200m.

Moored currents and wave measurements taken directly under hurricanes during their passage are difficult to obtain due to the unpredictability of the locations that hurricanes will appear and the paths they will follow. Most measurements of hurricanes have been chance encounters by instruments deployed for other scientific purposes, as was the case in this study. The relatively tight grid pattern, 30 km spacing, of the mooring array and the full water column measurements make this study ideal for investigating the oceanic response to a hurricane. The processes observed in the current velocity data collected during the hurricane include deterministic background tidal variability, background eddy fields circulation patterns associated with the Loop Current and eddies at the time of the storm, and near inertial and sub-inertial variability that is initiated as a response to the storm. Many studies have investigated the oceanic response to hurricanes captured by moored arrays in the Gulf of Mexico (Brooks 1983, Shay, Elsberry, and Black 1989, Teague et al. 2007, Zheng et al. 2006, Hamilton 1990).

The surface circulation patterns in the Gulf of Mexico include a western boundary current and general anticyclonic circulation, with water entering the Gulf through the Yucatan Strait between the Yucatan Peninsula of Mexico and Cuba as shown in the mesoscale altimetry figure for the Gulf of Mexico (Figure 2). Warm water enters the Gulf of Mexico then flows northward before sharply turning east and southeast to exit through the Florida Straits (Stommel 1958).

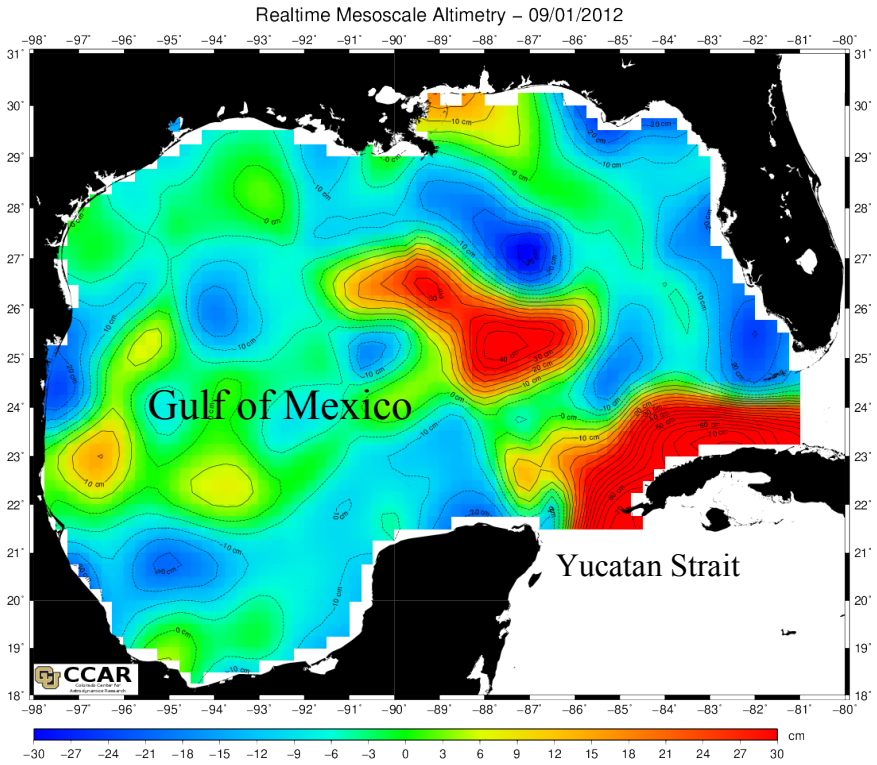


Figure 2. Realtime Mesoscale Altimetry for 09/01/2012. This altimetry figure shows the location of the loop current and eddies in the Gulf of Mexico. (Source: Dr. Robert Leben at the Colorado Center for Astrodynamics Research at the University of Colorado Boulder.)

The sharp turn to the right of the warm water mass after it enters through the Yucatan Strait produces the characteristic Loop Current that is responsible for the many of the upper ocean circulation patterns in the Gulf of Mexico. As the Loop Current extends farther north, anticyclonic warm core eddies are periodically shed that migrate westward across the Gulf of Mexico. Eddies can impact tropical storm events in the Gulf of Mexico by affecting the amount of thermal energy in the upper ocean available for the storm (Jaimes and Shay 2009, 2010).

The deep circulation in the Gulf of Mexico has been relatively less studied than the surface circulation due in part to the relative difficulty in instrumenting the area and the relative lack of long-term data collected at depth. Hamilton (1990) reported one of the earliest widespread data collection and analysis of deep-water currents. This study featured current measurements collected from 3 moored arrays deployed below 1000m in the eastern, central, and western Gulf of Mexico. The study determined that motions having the characteristics of Topographic Rossby Waves dominate the current variability in the lower regions of the Gulf of Mexico. Topographic Rossby Waves, TRW, can be generated by the low frequency pulsations of the Loop Current and the periodic shedding of warm core eddies. It was also determined that the TRWs became more decoupled from the surface and upper layer currents as they propagated into the western basin (Hamilton 1990). Deep eddies (below 1000m) have also been shown to contribute to the shedding of surface eddies from the Loop Current that in turn excite TRWs that transfer energy to the northern slopes of the Gulf of Mexico (Oey 2008).

The local water properties including temperature, salinity and density structures are also important for understanding the oceanic response to a hurricane. The density structure of the water column combined with the circulation patterns can affect how energy can propagate through the water column after an extreme event such as a hurricane. The relative vorticity of the region can also affect the frequency of the inertial response to either above (in cyclonic background flow) or below (in anti-cyclonic flow) the local inertial frequency (Mooers 1975, Kunze 1985). The movement of a hurricane over a water mass has been shown to result in a well-observed asymmetrical sea surface

cooling where the right side of the hurricane track experiences a greater amount of heat loss compared to the left side of the storm track. This asymmetrical sea surface cooling implies a typical pronounced rightward bias in the current response (Church, Joyce, and Price 1989, Sanford et al. 1987, Shay et al. 1998, Shay et al. 1992). Numerical ocean models have been used to explain that the directions of the wind stress vectors are responsible for the pronounced rightward bias in the observed SST response to a hurricane (Bender, Ginis, and Kurihara 1993, Price 1983).

Strong near-inertial oscillations generated by storms have been observed in current meter data in the Gulf of Mexico, Atlantic, and Pacific (Brooks 1983, Qi et al. 1995, Shay and Elsberry 1987, Shay and Chang 1995, Shay et al. 1998). Sub-inertial oscillations (2-10 day periods) have been observed in moored current meter data in response to Tropical Cyclone Gonu in the Northern Arabian Sea (Wang et al. 2012) and sub-inertial oscillations with 2-5 day periods were observed in moored current meter data in response to Hurricane Ivan in the northeastern Gulf of Mexico (Teague et al. 2007).

The objective of this thesis is to provide a three-dimensional description of the full water-column oceanic response to Hurricane Isaac in September 2012 from data collected by a mooring array on the slope of the Northern Gulf of Mexico. I plan to describe the metrics of the oceanic response observed in the data including the vertical and horizontal propagation speeds of the near-inertial oscillations, the phase propagation directions of the oscillations, the group velocities of these waves, the relationships between the oscillations observed at different depth levels, and the difference in these

metrics relative to the position of the hurricane and its track. The relative vorticity of the region will also be calculated and used to evaluate the effect of vorticity on the current response to Hurricane Isaac. The goal of this research is to describe the impact of Hurricane Isaac on the physical structure of the Gulf of Mexico by determining the metrics of the storm's impact and comparing these metrics to previous observations.

This research is funded by the Gulf Integrated Spill Research Consortium as one of seven consortia funded by the Gulf of Mexico Research Initiative. A major goal of the Gulf Integrated Spill Research Project is to validate and improve oil spill transport and transformation prediction using the numerical circulation models that use data collected near the Deepwater Horizon oil spill site. The description of the oceanic response to a hurricane event will help to improve the model's capability to capture the near-inertial and sub-inertial response from future extreme events in the Gulf of Mexico by utilizing the metrics determined from Hurricane Isaac.

# 2. DATA AND METHODS

This section summarizes the GISR mooring deployment cruise and the hydrographic studies completed. Current meter data, hydrographic data, satellite altimetry derived sea surface height, and gridded wind model product used in this study are presented including the methods used to prepare each data set for further analysis. The analyses used in this study including wavelet analysis, coherency analysis, and spectral analysis will be described as well as the methods of calculation of relative vorticity and the derivation of hurricane parameters and hurricane response metrics.

## 2.1 Data

### 2.1.1 GISR Mooring Data

In July 2012, six deepwater current meter moorings, named M1 through M6, were deployed in the Mississippi Fan region of the northern Gulf of Mexico as part of the Gulf Integrated Spill Research Project (Table 1). One full water column mooring, M1, was deployed in 1690 m of water at 28 29.9957'N and 88 30.0043'W in close proximity to the location of the Deepwater Horizon oil spill site (Figure 3).

Each mooring featured an upward-looking 75-kHz Acoustic Doppler Current Profiler, ADCP, along with other oceanographic sensors measuring currents, pressure, temperature, and conductivity (Figure 4). Table 1lists each of the deployed sensors and the depths of deployment for each mooring. Figure 5 shows the engineering schematics, not to scale, for the full water-column mooring measuring 1000 m in length (left) and the shorter moorings each measuring 500 m (right).

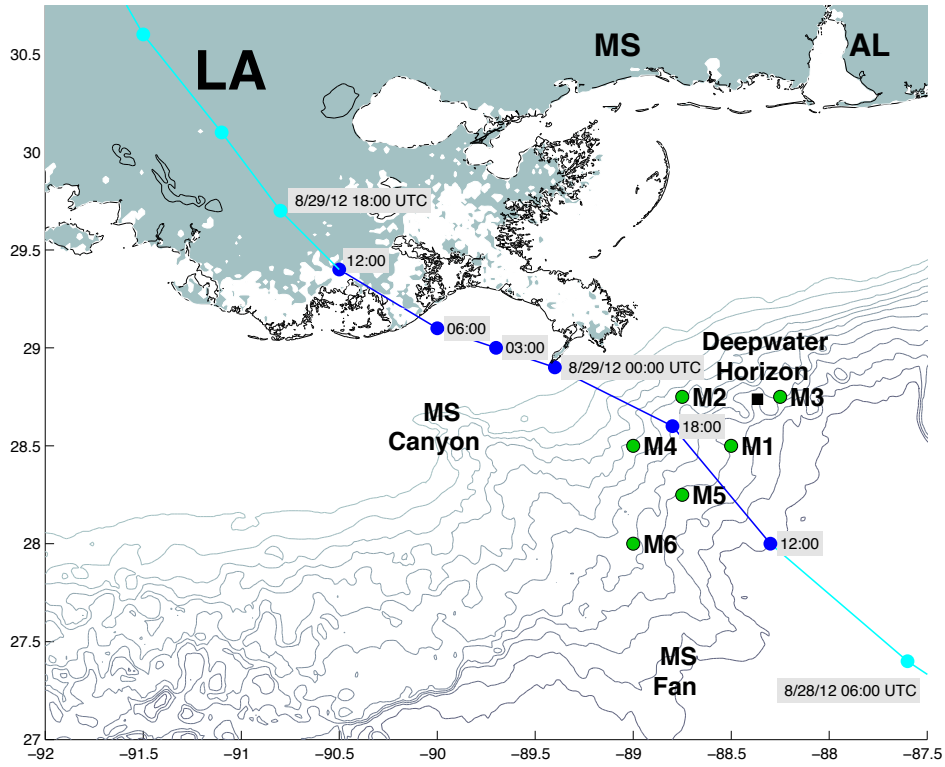


Figure 3. Hurricane Isaac Storm Track over GISR Mooring Array. This basemap shows the GISR mooring locations (green circles) in the Gulf of Mexico and the Deepwater Horizon site (black square). Storm track positions are shown as circles with connecting lines representing when the storm was a hurricane (blue) and when Isaac was classified as a tropical storm (cyan). Bathymetry lines are shown every 200 m starting at 200 m and ending at 2200 m.

Each RDI 75 kHz LongRanger ADCP reported data at 30-minute intervals with a total of 12 pings per ensemble from a total of 37 bins with bin sizes of 16 meters. All other instrumentation had averaging intervals of 1 hour. All six ADCPs were successfully recovered and recorded data from deployment to recovery. Two of the four InterOcean S4As on Mooring 1 failed in September 2012, with the shallowest S4A failing on 6 September 2012 and the next shallowest S4A failing on 27 September 2012.

Difficulties with the recovery of Mooring 2 resulted in the loss of two temperature sensors and two RCM current meters as well as a SBE-37 Microcat CTD (conductivity, temperature and depth). The quality control protocols will be discussed in Section 2.2.1. The ADCP current and pressure records from each mooring as well as the InterOcean S4As and the RCM current records will be used in this study.

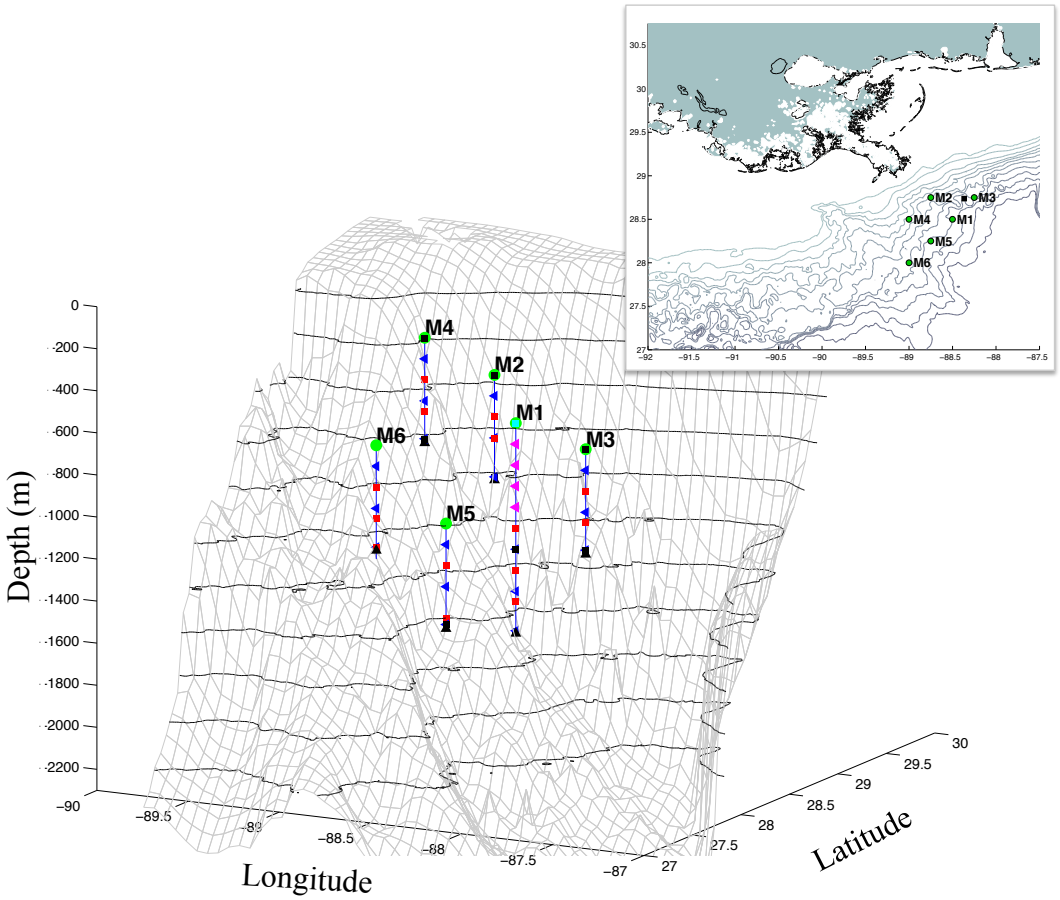


Figure 4. 3D Basemap of GISR Mooring Array. M1 (28.5'N, 88.5'W), M2 (28.75'N, 88.75'W), M3 (28.75'N, 88.25'W), M4 (28.5'N, 89'W), M5 (28.25'N, 88.75'W), M6 (28'N, 89'W). Green circles are the upward looking 75kHz ADCPs. The inset basemap shows the location of the mooring array relative to the coastline. Bathymetry lines are shown every 200 m beginning at 200 m and ending at 2200 m for both the 3D and inset basemaps.

| Mooring | Latitude | Longitude | Total Water Depth | 75kHz ADCP | SBE-16 CTD | InterOcean S4A | StarMon Temp | RCM-8 | RCM-11 | SBE-37 Microcat | Benthos 685A |
|---|---|---|---|---|---|---|---|---|---|---|---|
| | | | | Depth | Depth | Depth | Depth | Depth | Depth | Depth | Depth |
| 1 | 28.50N | 88.50W | 1690m | 690m | 692m | 790m | 1190m | | 1290m | 1292m | 1690m |
| | | | | | | 890m | 1390m | | 1490m | 1679m | 1690m |
| | | | | | | 990m | 1540m | | 1677m | | |
| | | | | | | 1090m | | | | | |
| 2 | 28.75 N | 88.75 W | 1035m | 535m | | | *735m* | | *635m* | *537m* | 1035m |
| | | | | | | | *837m* | | *835m* | 1022m | 1035m |
| | | | | | | | | | 1020m | | |
| 3 | 28.75 N | 88.25 W | 1337m | 837m | | | 1037m | | 937m | 839m | 1337m |
| | | | | | | | 1187m | | 1137m | 1319m | 1337m |
| | | | | | | | | | 1317m | | |
| 4 | 28.50 N | 89.00 W | 836m | 336m | | | 536m | | 436m | 338m | 836m |
| | | | | | | | 686m | | 636m | 818m | 836m |
| | | | | | | | | | 816m | | |
| 5 | 28.25 N | 88.75 W | 1650m | 1150m | | | 1350m | 1450m | 1250m | 1632m | 1650m |
| | | | | | | | 1500m | | 1630m | | 1650m |
| | | | | | | | | | | | |
| 6 | 28.00 N | 89.00 W | 1312m | 812m | | | 1012m | 1112m | 912m | | 1312m |
| | | | | | | | 1162m | | 1297m | | 1312m |
| | | | | | | | 1299m | | | | |

Table 1. Mooring Instruments and Deployment Depths. Mooring locations and instruments deployed are listed, including the water depth of each instrument. Italicized depths indicate instruments that were lost due to complications with mooring recovery. Highlighted depths indicate instruments that are used in this study. Each 75-kHz ADCP had a sampling rate of 30 minutes, and all other instruments had sampling rates of 1 hour.

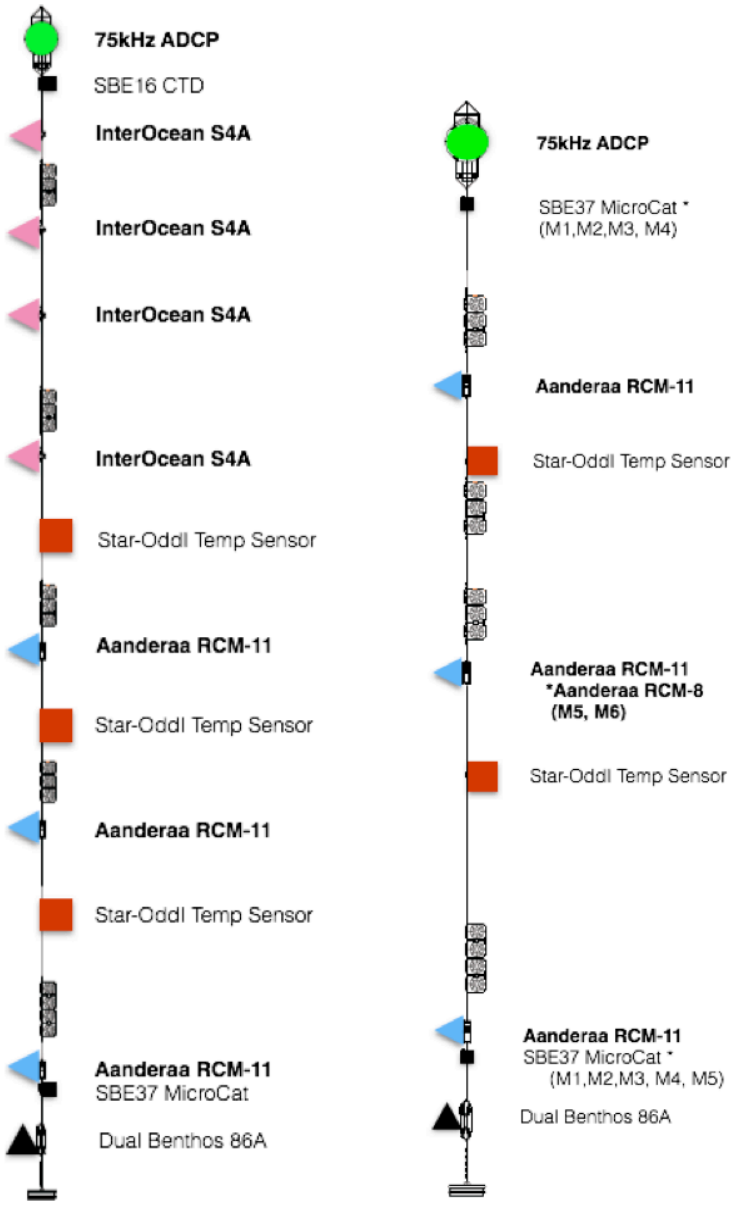


Figure 5. Schematics for GISR Moorings. Mooring schematics are shown for full water-column mooring (left) and shorter moorings (right). Instruments are labeled with shapes and colors corresponding to the 3D mooring basemap (Figure 4). Drawings are not to scale. Schematic drawings courtesy of J. Walpert, Geochemical and Environmental Research Group/Texas A&M University.

### 2.1.2 Gulf Integrated Spill Research Cruise CTD Data

In July 2012, the GISR mooring deployment cruise, G01, was conducted in the Mississippi Fan region of the Gulf of Mexico. A mooring recovery cruise, G04, was conducted the following year in the same region. CTD (conductivity, temperature and depth) profiles from a SeaBird 911*plus* were collected in a grid pattern around the mooring deployment site during both cruises as shown in Figure 6.

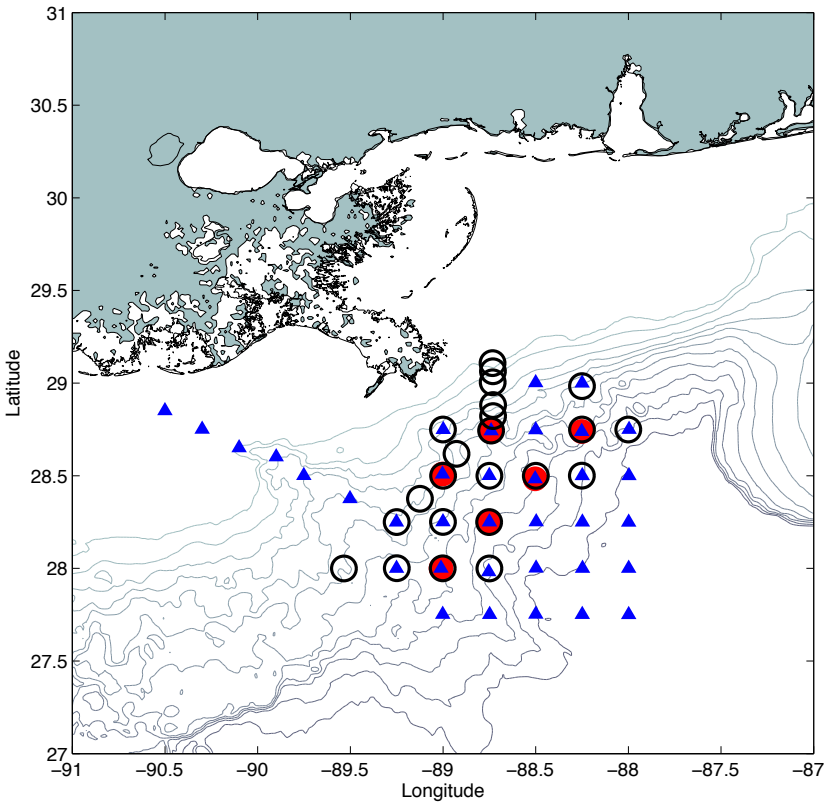


Figure 6. GISR CTD Station and Mooring Array. This basemap shows the location of GISR moorings (red circles), G01 CTD stations in 2012 (blue triangles) and G04 CTD stations in 2013 (black rings). Bathymetry lines are shown every 200m beginning at 200 m and ending at 2200m.

Processing of the CTD profiles was done using Sea Bird's Seasave Win32 program, version 7.0. Each profile underwent quality control procedures that included removing extreme outliers and flagged data points. The temperature and salinity relationship for each cast taken during the July 2012 G01 mooring deployment cruise are shown in left panel of Figure 7. The right panel shows the temperature and salinity relationship for the G04 mooring recovery cruise one year after the deployment cruise in July 2013. The color of each data point represents the measured dissolved oxygen concentration. The salinity, temperature and density structures of the water column derived from the conductivity, temperature and pressure profiles from the G01 cruise will be used to determine the stratification profiles ($N^2$) and depths of the mixed layer and thermocline before the hurricane. The temperature and salinity data from the G01 cruise CTD casts are used to determine the stratification of the water column by calculating the average Brunt–Väisälä frequency in the region of the moorings. The method for derivation and application of the Brunt–Väisälä frequency estimations will be discussed in Section 2.2.10.

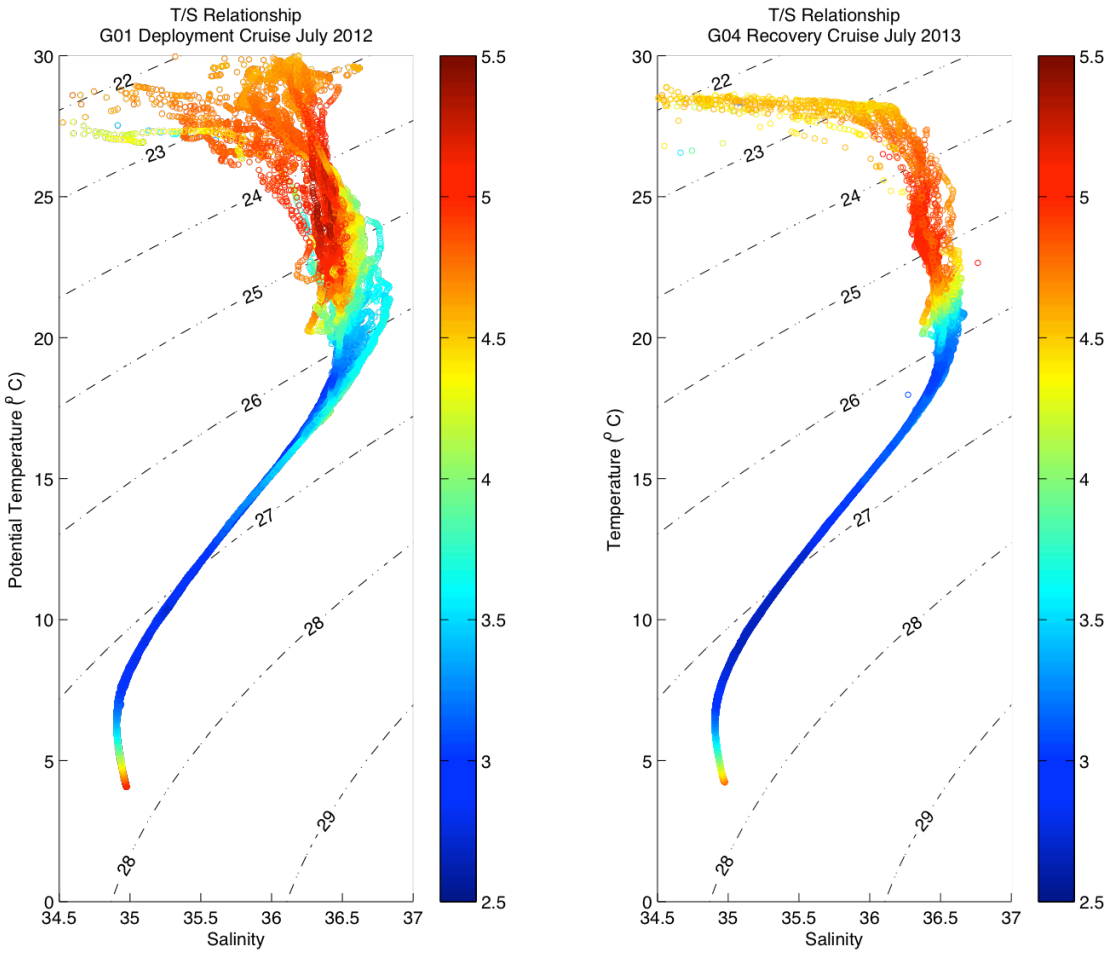


Figure 7. Temperature-Salinity for GISR CTD Data. The Temperature-Salinity Diagrams are shown for CTD data collected on G01 mooring deployment cruise in early July 2012 (left) and the CTD data collected on G04 mooring recovery cruise in early July 2013 (right). The black contour lines show the density isopycnals in kg/m$^3$. The colors represent dissolved oxygen concentrations.

### 2.1.3 Hurricane Track Data

Best track hurricane storm path data and observations of wind and pressure were obtained from ftp://ftp.nhc.noaa.gov/atcf/archive/2012/ as reported by the National Hurricane Center in the Tropical Cyclone Report of Hurricane Isaac (Berg 2013). The reported wind speed and surface pressure data are a best fit calculated from observations

of the hurricane from satellites, aircraft, and radar, ships, land stations and buoys. Doppler radar data from the National Weather Service, Météo-France, and the Institute of Meteorology of Cuba were used to make center fixes and help track the center of Isaac through the Gulf of Mexico. The event of Hurricane Isaac's passage over the mooring array can be partitioned into 3 stages, the pre-storm period, the storm's passage, and the relaxation stage or wake of the storm that begins immediately after the passage of the storm and lasts for approximately 10-15 days after the storm.

### 2.1.4 Model Wind Output

Output from a ROMS forced atmospheric model was obtained for estimating wind stress and wind stress curl near the mooring site and on each side of the hurricane track around the time of Hurricane Isaac. The wind stress values will be used to help determine metrics for the storm. The model output was 6-hourly *u* and *v* wind velocity components in m/s analyzed 10 m about the sea surface starting on 1 July 2012 and running until 31 October 2012.

## 2.2 Methods

### 2.2.1 Quality Control and Interpolation

The entire yearlong ADCP and current meter records from the GISR moorings were rigorously quality controlled (J. Kuehl, unpublished) in accordance with the procedures outlined in the MMS Quality Control Analysis report for ADCP data (Bender and DiMarco 2009). The quality-controlled data were originally recorded at 30-minute intervals from the ADCPs and at hourly intervals from the other current meters. After quality control procedures including the removal of flagged data, the removal of extreme

outlier and gap filling were applied to each data set, all records were subsampled using linear interpolation to a consistent hourly grid to allow for comparison between records.

### 2.2.2 Detiding

The moorings were deployed near a critical latitude, defined as 30° N or S, meaning that local inertial period, approximately 24 hours, is very near the local diurnal tidal period. This makes detiding data collected in this region more difficult, since simple low pass filtering cannot separate the inertial and tidal energy. Harmonic analysis is used to remove the tidal frequencies as described in DiMarco and Reid (1998). The quality-controlled data are detided to remove the eight principal tidal constituents using the iterated least squares method of cyclic descent (Bloomfield 1976, DiMarco and Reid 1998). Due to the extreme hurricane event in this relatively short time series, the currents recorded during the storm event were identified and removed before fitting the tidal oscillations to the time series. The frequency of the inertial oscillations induced by the storm is closely aligned with the frequency of the local diurnal tidal oscillations. If the hurricane event were not removed from the record prior to analysis, the larger amplitudes of the inertial oscillations would mask the smaller tidal amplitudes resulting in an inaccurate evaluation of the tidal energy in the velocity records.

### 2.2.3 Filtering

Once the tides are removed from the time-series current velocity data, a cosine-Lanczos filter will be used to obtain band passed records of the data (Emery and Thomson 2001). The cosine-Lanczos filters applies a weighted sine function to the time-series data in order to obtain each low passed data record (Duchon 1979). A 40-hr LP

filter will be applied to each of the velocity data records to remove tidal and inertial variability. The 40-hr LP filtered data were used to identify and quantify the sub-inertial oscillations present in each record using wavelet analysis. Band-passed records were obtained by subtracting a lower frequency low-passed record from a higher frequency low-passed record. All data records were band-pass filtered between .8*f* to 1.2*f*, with *f* being the local Coriolis parameter, to isolate the near inertial energy band. A 2-5 day period band and a 5-12 day period band were partitioned from each time series to isolate the corresponding sub-inertial wave that is observed in the time series records.

**2.2.4 Wind Stress Curl**

Output from the atmospheric model was used to calculate wind stress and wind stress curl for the storm track (near Mooring 1) and on each side of the hurricane track. First, wind speed was calculated from the velocity components using the Pythagorean theorem, and the neutral wind drag coefficient was estimated to range between .0011 and .002 using the method of Large and Pond (1981). The zonal and meridional wind stress components were calculated according to the equation presented by Nelson and United States National Marine Fisheries Service (1977)

$$(\tau_x, \tau_y) = \rho_a C_D ( |W_{10}| U_{10}, |W_{10}| V_{10} ),$$

where $\rho_a$ is the density of air (1.22 kg/m$^3$), $C_D$ is the drag coefficient, $W_{10}$ is the wind speed in m/s, and $U_{10}$ and $V_{10}$ are the eastward and northward components of the wind velocity measured at a height of 10 m obtained from the model output. The resulting wind stress components were used to compute the curl of the wind stress at the mooring site and on each side of the storm track as shown in Figure 8. The wind stress and wind

stress curl time series (yellow crosses in Figure 8) were calculated for the mooring area at the location of Mooring 1 (28.5'N, 88.5'W), for the right side of the storm 102 km northeast of Mooring 1 at (27.75'N, 89.25'W), and for the left side of the storm 102 km southwest of Mooring 1 at (29.25'N, 87.75'W).

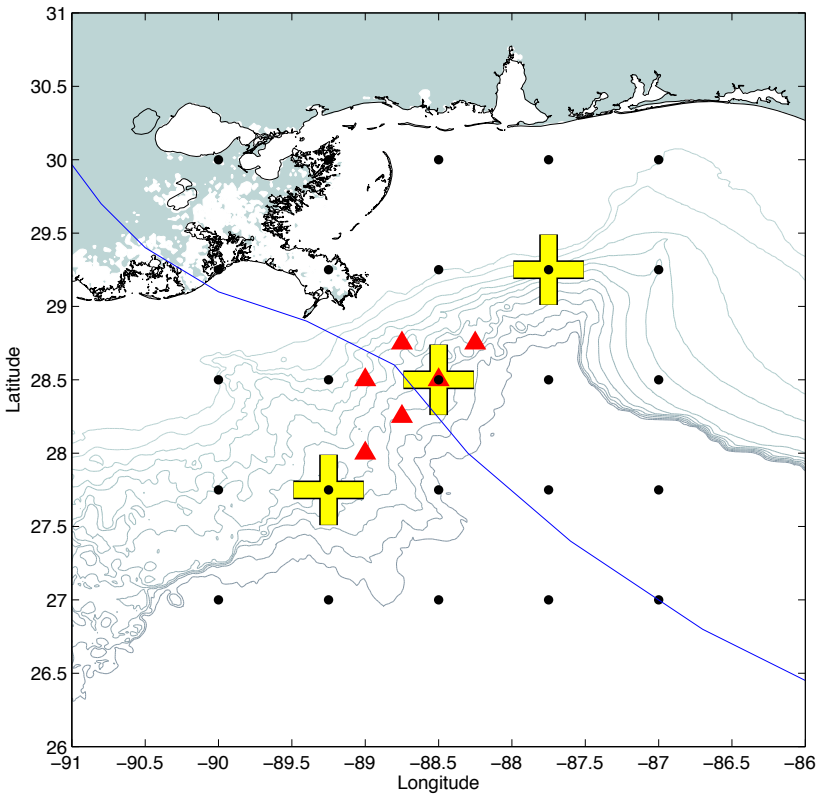


Figure 8. Model Output Locations near GISR Mooring Array. This basemap shows mooring locations (red triangles) and locations of wind speed estimates from model output (black dots). The blue line shows the storm path of Hurricane Isaac. The yellow crosses show the locations for the estimation of wind stress curl calculated from wind model output. Bathymetry lines are shown every 200 m beginning at 200 m and ending at 2200 m.

### 2.2.5 Wavelets

Wavelet analysis is used to isolate the localized variations of frequency within a time series record. The wavelet analysis software package developed by Torrence and Compo (1998) will be used to perform wavelet transforms on current velocity records. The software package can be found at http://paos.colorado.edu/research/wavelets/. A Morlet basis function is used to generate wavelet power spectra for each ADCP and current meter record. Scale averaged wavelet power in the inertial band (.8*f* to 1.2*f*) and the sub-inertial bands (2-5 days and 5-12 days) are generated to provide a temporally localized estimate of amplitude and phase of the energy in each band. Figure 9 shows the wavelet analysis output for 300m at Mooring 1 during the passage of Hurricane Isaac. Hovmöller diagrams, space-time plots, of scale averaged wavelet power amplitudes in the inertial and sub-inertial band are created to show the change in variance over time and depth. A correction to the original software package is applied as suggested in Liu, Liang, and Weisberg (2007) to more accurately estimate the wavelet spectrum by rectifying a bias for low frequency data records.

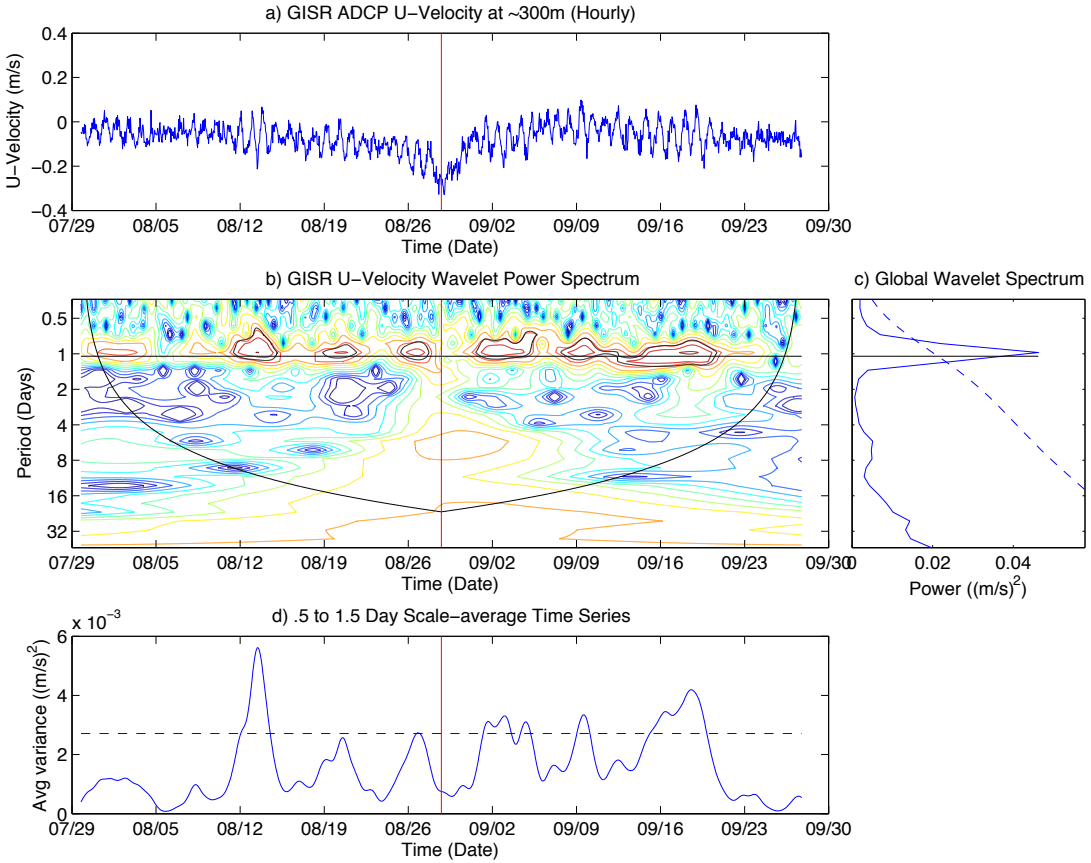


Figure 9. Wavelet Analysis Example for Mooring 1 at 300m. The wavelet of Mooring 1 for hourly u-velocity data collect at 300 m depth is shown. The time series is centered near the hurricane's closest approach to the mooring, with one month before and after the storm displayed. Figure 9a displays the detided and linearly interpolated time series before wavelet analysis. Figure 9b shows the Wavelet Power Spectrum. Figure 9c displays the Global Wavelet Spectrum, which is the horizontal integration of the wavelet power from Figure 9b. Figure 9d shows the scale-averaged time series for the .5-2 day period band, which is also a vertical integration within this inertial band.

### 2.2.6 Wavelet Coherence Analysis

Coherence is the measure of correlation between independent data set by frequency. Coherency analysis is used to quantify correlation and lag as a function of frequency. Coherence analysis determines if current velocities between any two signals are correlated or if the phase is lagging (Emery and Thomson 2001). The following equation is used to estimate the 95% confidence level:

$\gamma 2 = 1-\alpha\ [2/(DOF-2)]$ (Thompson 1979), with DOF being the degrees of freedom. Wavelet coherence analysis utilizes a cross wavelet transform and wavelet coherence to examine relationships in time frequency space between two time series. The cross wavelet transform exposes regions with high common power and further reveals information about the phase relationship between two signals. If two signals share a large common power and have a consistent phase relationship then a possible causality between the time series is suggested (Grinsted, Moore, and Jevrejeva 2004).

In this study, wavelet coherence analysis will be used to compare two velocity time series records at a specific location or a similar depth level in order to determine periods of strong coherency and phase differences between the two records. Figure 10 shows an example of the wavelet coherence between the 600 m records at Mooring 1 and Mooring 3. Strong coherence (correlation above 0.8) is observed in the near-inertial range after the passage of Hurricane Isaac. Coherence (correlation above 0.7) between the two records is also observed at a period between 3 and 5 days at the time of the storm.

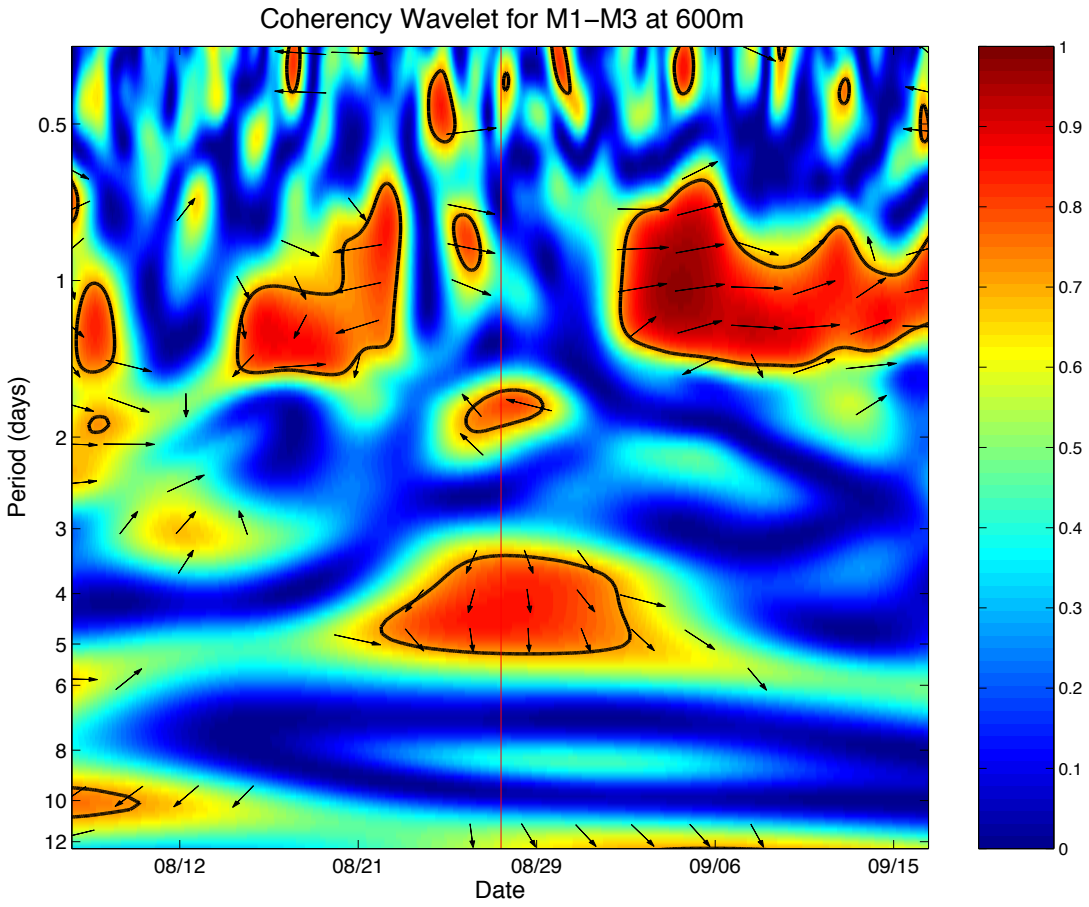


Figure 10. Wavelet Coherency Analysis for Mooring 1 and Mooring 3 at 600m. Coherency wavelet of the comparison between the 600 m u-velocity records at Mooring 1 and Mooring 3 is shown. The coherency wavelet shows the level of coherency found between the two records at each period over a period of 20 days before and after the nearest passage of Hurricane Isaac to the mooring array (red vertical line). The 5% significance level against red noise is shown as thick contour line. The relative phase relationship is shown as arrows (with in-phase pointing right, anti-phase pointing left, and M1 leading M3 by 90° pointing straight down).

### 2.2.7 Spectral Analysis

A common data analysis method involves identifying the variance in a spectral range of frequencies that are present in a time series since many geophysical temporal phenomena are inherently periodic. Spectral analysis is a technique applied to time series data that makes use of the Fourier transform, which assumes stationary power or amplitude, and partitions the variance in a record into different spectral bands based on frequency (Emery and Thomson 2001). Spectral bands for periods of $.8f$ - $1.2f$, 2-5 days, and 5-12 days will be of interest for this study to analyze the inertial and the sub-inertial frequencies found in each record. To perform the spectral analysis, Fast Fourier Transform (FFT) will be applied to each data record following Welch's method (Welch 1967).

### 2.2.8 Relative Vorticity

Relative vorticity is the measure of the rotation of the ocean relative to the background vorticity due to the rotation of the Earth, or planetary vorticity. The definition of relative vorticity is $\zeta = \delta v/\delta x - \delta u/dy$, where $u$ and $v$ are the velocity components in the $x$ and $y$ directions respectively (Emery and Thomson 2001). Regions of positive relative vorticity in the ocean correspond to cyclonic circulation in the Northern Hemisphere, and regions of negative relative vorticity correspond to anticyclonic circulation.

Relative vorticity for the right side of the hurricane track is calculated from current meter data at Moorings 1, 2 and 3 at all available depths between 245 m and 452 m. Due to the deep deployment of Mooring 5 in contrast to Moorings 4 and 6, the

current meter records from Mooring 4 and 6 are used with Mooring 1 to estimate the relative vorticity on the left side of the storm track at all available depths between 187 m and 291 m as well as 436 m and 636 m. The relative vorticity is calculated hourly for a triangular array by approximating the circle integration by a discrete sum of the radial and normal velocity components along the circle connecting the three moorings according to the methods described in Muller, Lien, and Williams (1988). The relative vorticity estimates for each side of the hurricane will be compared with altimetry records and current meter records to determine how relative vorticity relates to oceanic response to Hurricane Isaac.

**2.2.9 Hurricane Parameters**

Hurricanes can be described by a few fundamental variables. These include the average translation speed of the storm $U_h$, the radius of maximum wind speed $R_{max}$, the maximum wind stress $\tau$, the inertial frequency of the region *f*, and the reduced gravity g' (Price et al, 1994). Several non-dimensional parameters can also be derived from these fundamental variables in order to describe the oceanic response to the storm. These parameters include the non-dimensional storm speed S, the thermocline Burger number, B, and the Rossby number for the mixed layer current, Q.

$$S = \pi U_h / 4 f R_{max} \quad (1)$$

$$B = g' h_1 / 4 f^2 R^2_{max} \quad (2)$$

$$Q = \tau / \rho_o h_1 U_h f \quad (3)$$

where

$U_h$ = storm translation speed,

$\rho_o$ = density of seawater,

$h_1$ = depth of mixed layer,

$\tau$ = max wind stress,

$f$ = local Coriolis frequency.

The non-dimensional storm speed, S, is the ratio of the local inertial period to the hurricane residence time. The thermocline Burger number, B, is a direct measure of the pressure coupling between the mixed layer current and the thermocline current. The Rossby number, Q, is the ratio of horizontal advection of momentum to the Coriolis force. The derivations of these non-dimensional parameters are described in Price et al. (1994). These variables and parameters determined for Hurricane Isaac will be compared with those reported for other hurricanes.

**2.2.10 Water Column Response**

The measure of stratification or stability in the water column is important to determine the group velocities of the inertial response to Hurricane Isaac. The Brunt–Väisälä frequency ($N$), or buoyancy frequency, is the natural frequency of oscillation of a parcel of water displaced vertically from its level of equilibrium. In the ocean, larger values of $N$ correspond to a more stable water column. The Brunt–Väisälä frequency is defined as

$$N = \sqrt{-(g/\rho)*(\delta\rho/\delta z)}, \qquad (4)$$

where g is gravity, $z$ is depth, and $\rho$ is the potential density calculated using the potential temperature, salinity and pressure profiles.

A total of 36 CTD casts were taken on the G01 cruise. Of these, 18 casts were taken within 25 km of any mooring deployment site. These 18 casts are used to estimate the stratification of the water column before the passage of the hurricane. The Brunt–Väisälä frequency will be used with estimations of vertical and horizontal scales to calculate group velocities of near inertial oscillations observed in the wake of Hurricane Isaac.

Estimations of the vertical and horizontal scales of the near-inertial oscillations are determined by observing the phase shift of current meter amplitudes between different depth levels at a single mooring, and between similar depth levels from two separate moorings respectively. The speed of the energy propagation is determined by dividing the phase shift measured in time units by the known distance between the observations. When the frequency of the energy is known (i.e. the effective frequency) and the speed of the energy is calculated from the known distance traveled over time, the scale (or wavelength) is determined from speed = frequency x wavelength.

Using the vertical and horizontal scale estimates, the horizontal and vertical group speeds for the near-inertial response are calculated using equations 5a and 5b from Brooks (1983). For $N^2$ constant, we can determine the group speeds, or energy transport velocity vectors:

$$C_{gy} = \omega l^{-1} (N\omega^{-1} \tan\theta)^2, \quad (5a)$$

$$C_{gz} = -\omega m^{-1} (N\omega^{-1} \tan\theta)^2, \quad (5b)$$

in terms of the phase velocity vector,

$$C_p = (\omega l^{-1}, \omega m^{-1}), \quad (6)$$

where ω is the effective Coriolis frequency and *l* and *m* are the horizontal and vertical wavenumbers calculated from the length scales as

$$(l,m) = 2\pi(L_y^{-1},L_z^{-1}). \quad (7)$$

*N* is the estimated Brunt–Väisälä frequency calculated from the CTD profiles taken during the mooring deployment cruise. The tilt of the phase distribution with depth, or the angle between the phase vectors and the vertical, θ, can be determined directly from the length scales as

$$\tan\theta = lm^{-1} \quad (8)$$

and estimated from the dispersion relation as,

$$\tan\theta = N^{-1}(\omega^2 - f^2)^{1/2}, \quad (9)$$

where ω is the observed frequency of the near inertial response and *f* is the Coriolis parameter. As explained in Brooks (1983), depth-leading phases are indicative of downward propagation of energy into the thermocline. From (5b), the kinetic energy propagates vertically with the opposite sense of the phase propagation. In order for energy to propagate downward into the thermocline, the phase vector must be tipped slightly out of the vertical.

# 3. RESULTS

This chapter begins with a description of the actions of Hurricane Isaac in the Gulf of Mexico followed by the presentation of the hurricane data and parameters derived as described in the Section 2. The following section is a description of the physical processes recorded in the current meter data from the mooring array. This is accomplished through the examination of the time series, basic statistics and spectra of the velocity components from the available depths in the water column and the comparison to the sea surface height data for the study region.

The estimates of Brunt-Väisälä frequency, relative vorticity and wind stress curl for the study region will be presented in this section followed by the examination of the current response and variance observed during the passage and wake of the storm. The oceanic response to Hurricane Isaac will be the main focus of this section. The results from the analysis of the near-inertial and sub-inertial water column responses will be highlighted with an emphasis on the observed frequency shift and estimated group speed and propagation directions of the energy from the storm.

## 3.1 Hurricane Isaac

Tropical Storm Isaac entered the Gulf of Mexico on 27 August 2012 through the Florida Straits and strengthened to become a Category 1 hurricane around 1200 UTC 28 August when the eye of the storm was centered approximately 13 km southeast of the mouth of the Mississippi River. Hurricane Isaac passed directly over the center of the mooring array before making its first of two landfalls along the coast of Louisiana, the

first at Southwest Pass at around 0000 UTC on 29 August, then again just west of Port Fourchon, Louisiana approximately 8 hours later. Maximum sustained wind speeds of 129.64 km/hr were recorded with Hurricane Isaac's first landfall at Southwest Pass (Berg 2013). The translation speed of Hurricane Isaac as it passed over the mooring array was approximately 3.5 m/s based on reported times and locations of the center of the storm. Figure 11a shows the storm track of Isaac in the Gulf of Mexico, and Figure 11b shows the path of Hurricane Isaac as it passed over the GISR mooring array before and after making landfall. Figure 12 presents a time series of the reported storm wind speeds and sea level pressure and the calculated translation speeds during the storm's passage over the mooring array.

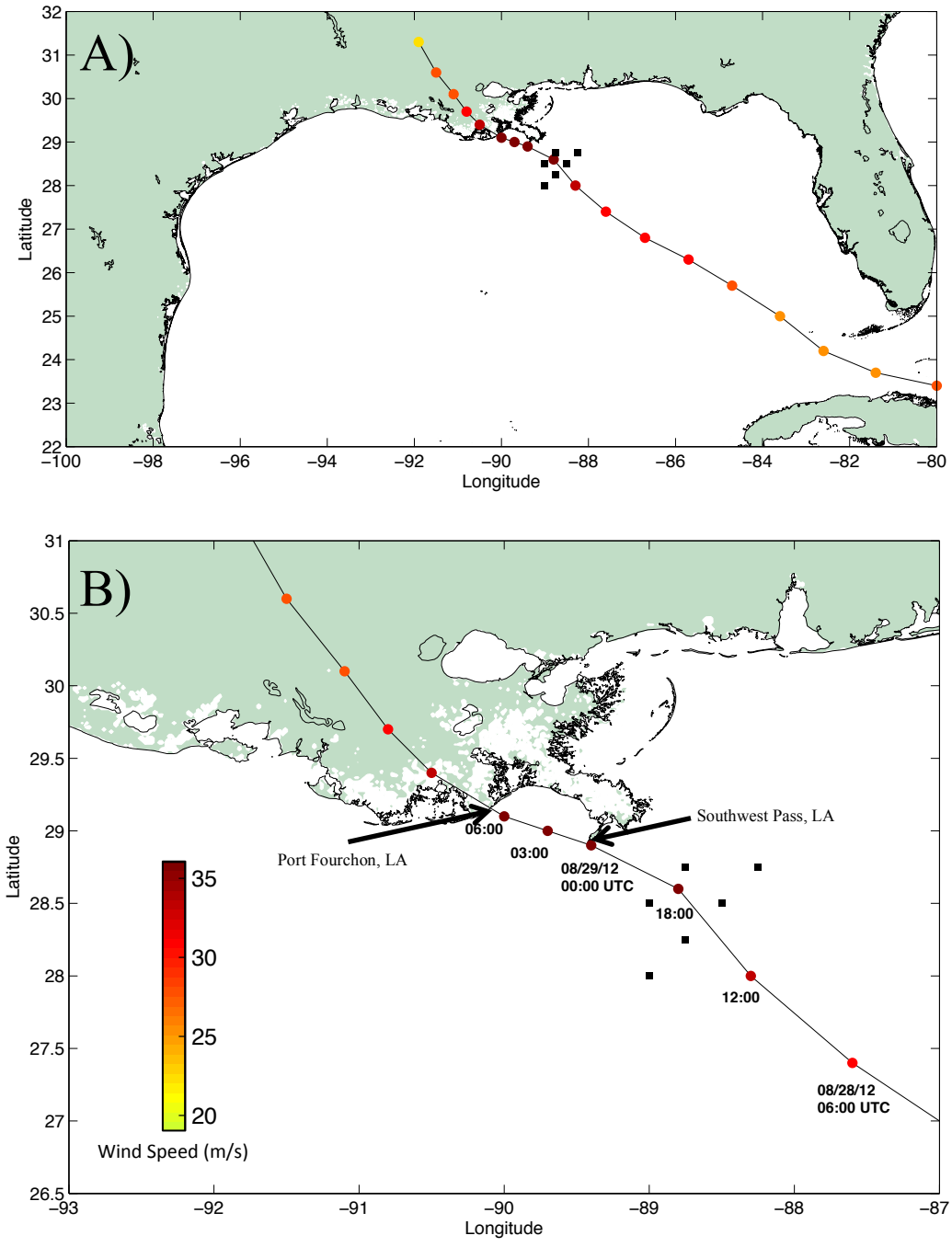


Figure 11. Hurricane Isaac Storm Track. (A) Storm track of Hurricane Isaac in the Gulf of Mexico, (B) Storm track of Hurricane Isaac over the GISR mooring array. Hurricane track points are colored according to reported wind speed in m/s.

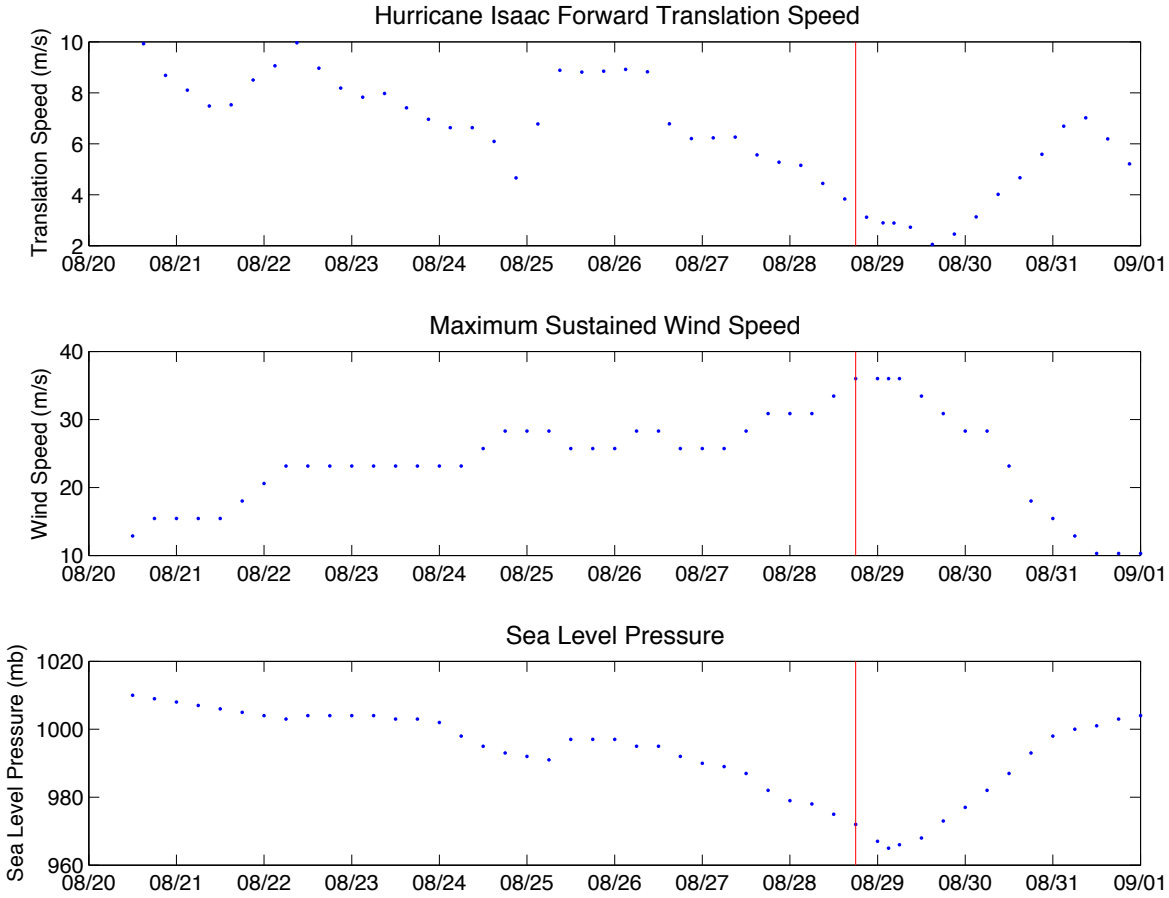


Figure 12. Hurricane Isaac Translation Speed, Wind Speed, and Sea Level Pressure. (A) Hurricane Isaac forward translation speed in m/s calculated from reported storm track positions; (B) Maximum sustained wind speed for Hurricane Isaac in m/s; (C) Sea level pressure during Hurricane Isaac. Red vertical lines represent closest approach of Hurricane Isaac to GISR mooring array. All times are reported in UTC. Storm track positions, wind speed and sea level pressure values were reported by Nation Hurricane Center and downloaded from ftp://ftp.nhc.noaa.gov/atcf/archive/2012/.

### 3.1.1 Scales and Parameters

The fundamental variables and the derived non-dimensional parameters as described in Section 2.2.9 for Hurricane Isaac are presented in Table 2. The same variables for Hurricanes Ivan, Norbert, Frederic, and Gilbert are also reported in Table 2. Hurricane Ivan struck the Gulf of Mexico in September 2004 as a Category 4 hurricane before making landfall near Gulf Shores, Alabama. Hurricane Ivan passed directly over a mooring array of 14 ADCPs deployed in the DeSoto Slope as part of the Slope to Shelf Energetics and Exchange Dynamics project conducted by the Naval Research Laboratory (Teague et al. 2007). Hurricane Norbert originated in the Pacific Ocean west of the Mexican coast and peaked in strength as a Category 4 hurricane before weakening back into a tropical storm and striking the Baja California Peninsula in September 1984. Aircraft deployed AXCPs captured currents near the storm's center providing a quasi-synoptic view of the response to Hurricane Norbert (Price, Sanford, and Forristall 1994). Hurricane Frederic struck the Gulf of Mexico as a Category 4 hurricane before making landfall near Dauphine Island, Alabama in September 1979. Hurricane Frederic passed within 80 km of an array of current meters in the DeSoto Canyon Region deployed by the U.S. Naval Oceanographic Office and within 150 km of an Ocean Thermal Energy Conversion mooring (Shay and Elsberry 1987). Hurricane Gilbert struck the western Gulf of Mexico in September 1988 and the primary dataset used to study the upper ocean response to the hurricane was acquired during five flights in which a number of AXBTs and AXCPs were deployed (Shay et al. 1992). The comparison of each of these storms to Hurricane Isaac in 2012 will be discussed later in the Chapter 4.

| Parameter | Isaac (2012) | Ivan (2004) | Norbert (1984) | Frederic (1979) | Gilbert (1988) |
|---|---|---|---|---|---|
| | | | | | |
| $U_h$ (translation speed) | 3.83 m/s | 5.8 m/s | 3.0 m/s | 6-7 m/s | 5.6 m/s |
| $R_{max}$ (cross track scale) | 92.6 km | 40 km | 20 km | 27-33 km | 60 km |
| $L_i$ (along track scale) | 55.03 km | 81 km | 62.5 km | -- | -- |
| $\tau_{max}$ (wind stress) | 1.35 $N/m^2$ | 6.7 $N/m^2$ | 4.0 $N/m^2$ | -- | 4.2 $N/m^2$ |
| f (Coriolis parameter) | 6.9 $x10^{-5}$ rad/s | 7.2 $x10^{-5}$ rad/s | 4.8 $x10^{-5}$ rad/s | 7.2 $x10^{-5}$ rad/s | 5.8 $x10^{-5}$ rad/s |
| g' (reduced gravity) | .04 $m/s^2$ | .04 $m/s^2$ | .04 $m/s^2$ | .022 $m/s^2$ | .0286 $m/s^2$ |
| $h_1$ (mixed layer depth) | 40-50 m | 50 m | 40 m | 40-50 m | 35 m |
| S (Non-dimensional Storm Speed) | 0.47 | 1.6 | 2.4 | 1.4 | 1.04 |
| B (Burger Number) | 0.009 | 0.06 | 0.37 | 0.08 | 0.08 |
| Q (Rossby Number) | 0.13 | 0.55 | 0.7 | -- | -- |

Table 2. Hurricane Parameters. Hurricane parameters for Isaac in 2012 calculated in the study, Ivan in 2004 (Teague et al. 2007), Norbert in 1984 (Price, Sanford, and Forristall 1994), Frederic in 1979 (Shay and Elsberry 1987), and Gilbert in 1988 (Shay et al. 1998) are presented.

### 3.1.2 Pre-Storm Conditions

40 HRLP velocity vector plots in Figure 13 show that in the pre-storm period currents at each mooring varied in direction, with upper ocean ($z < 200$ m) currents flowing to the north and northwest at Moorings 1 and 2 and currents flowing strongly to the south at Mooring 3. Currents directions and magnitudes at Moorings 4 and 6 varied before the storm. The current observations at all moorings are mostly consistent with the expected directions of the near -surface currents based on the available altimetry figures for the mooring area (Figure 14). The altimetry figures show a slight decrease in sea surface height that corresponds to a cyclonic feature in the area of the mooring array. This cyclonic feature is centered to the left side of the mooring array. The altimetry figures also show a slight increase in sea surface height on the right of the mooring array directly north of Mooring 3. A stronger cyclonic eddy is located to the southeast of the mooring array. The direction of flow observed at each mooring before the passage of the storm generally corresponds well with the expected flow directions based on the altimetry figures. The inconsistencies, particularly at Mooring 4, may be due to the low level of spatial and temporal resolution of the altimetry figures. Each altimetry figure is a composite of 14 days of satellite data combined with a model of the mean sea level for the Gulf of Mexico therefore inaccuracies over such a small spatial scale as the moorings compared to the entire Gulf of Mexico are to be expected.

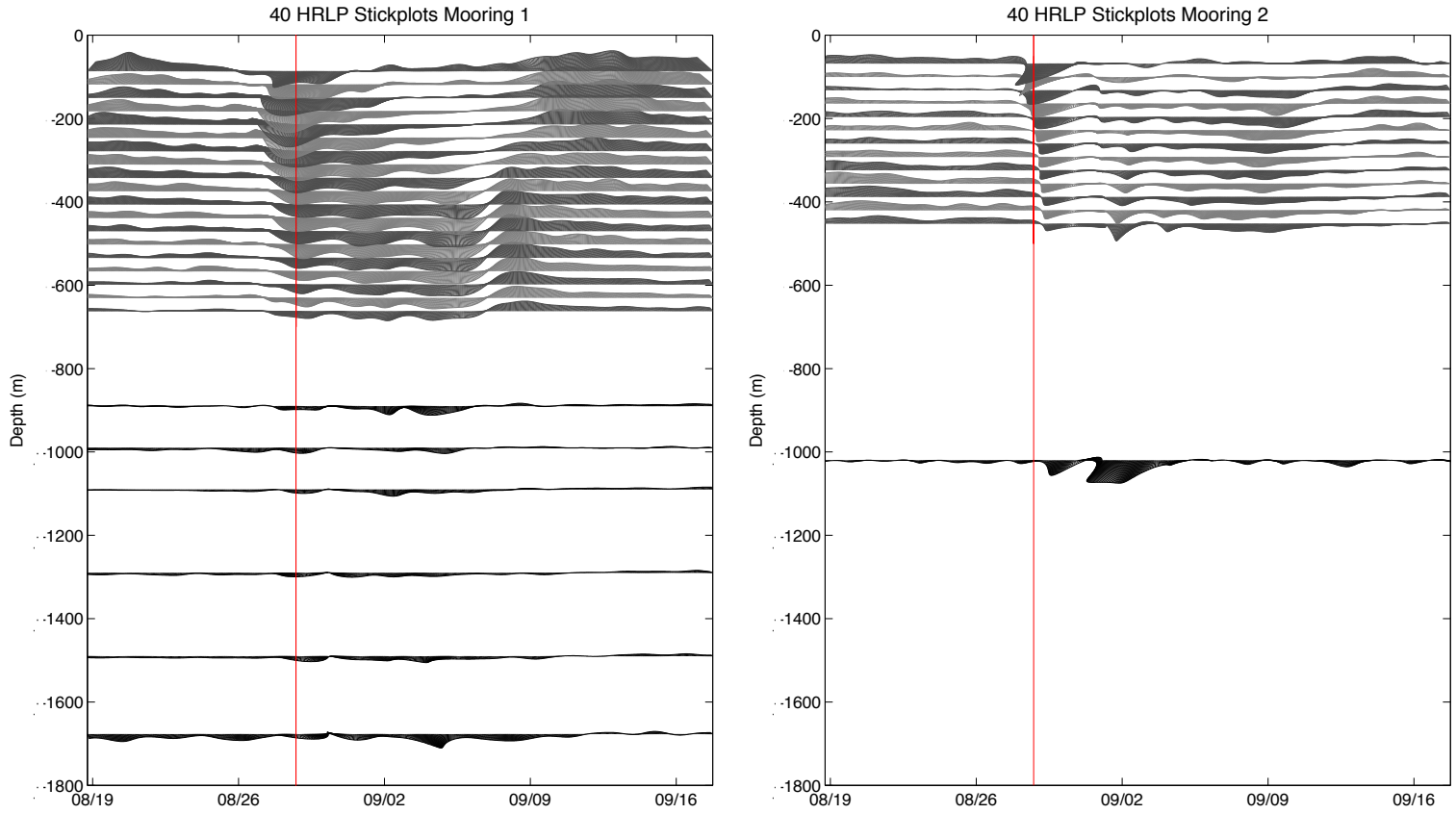


Figure 13. 40-hr LP Velocity Vector Plots. Velocity vector plots for 40 hour low passed current meter data at each mooring 10 days before and 20 days after the passage of Hurricane Isaac are shown. The vertical red line represents the closest approach of Hurricane Isaac on August 28, 2012 at 18:00 UTC. The ADCP data is show in alternating gray scale to provide contrast between depth layers. The black lines represent data from RCM and S4A instruments on each mooring. The direction of the vectors is oceanographic convention with currents pointing up on the page referring to currents coming from the south and flowing north.

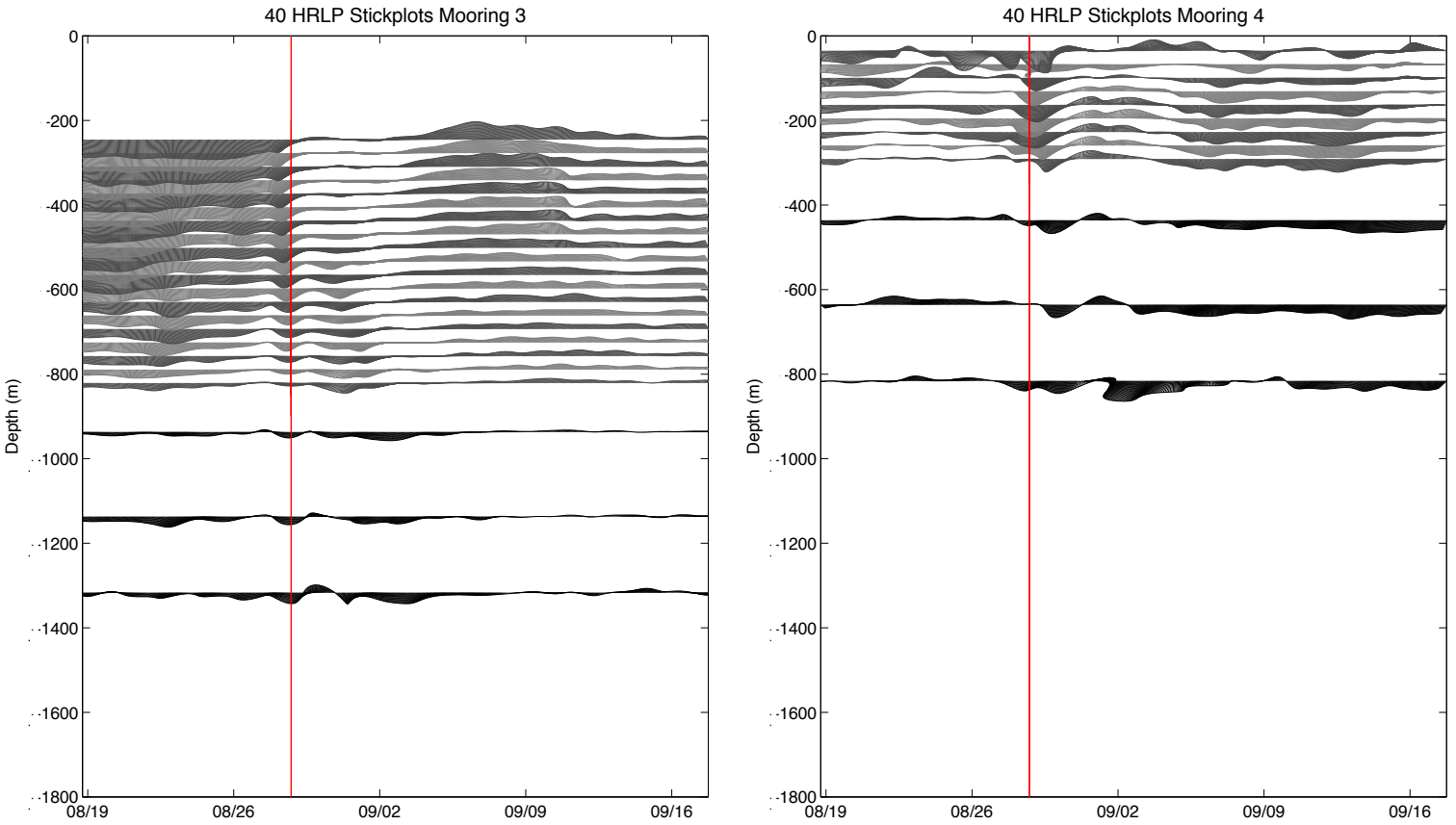


Figure 13 continued.

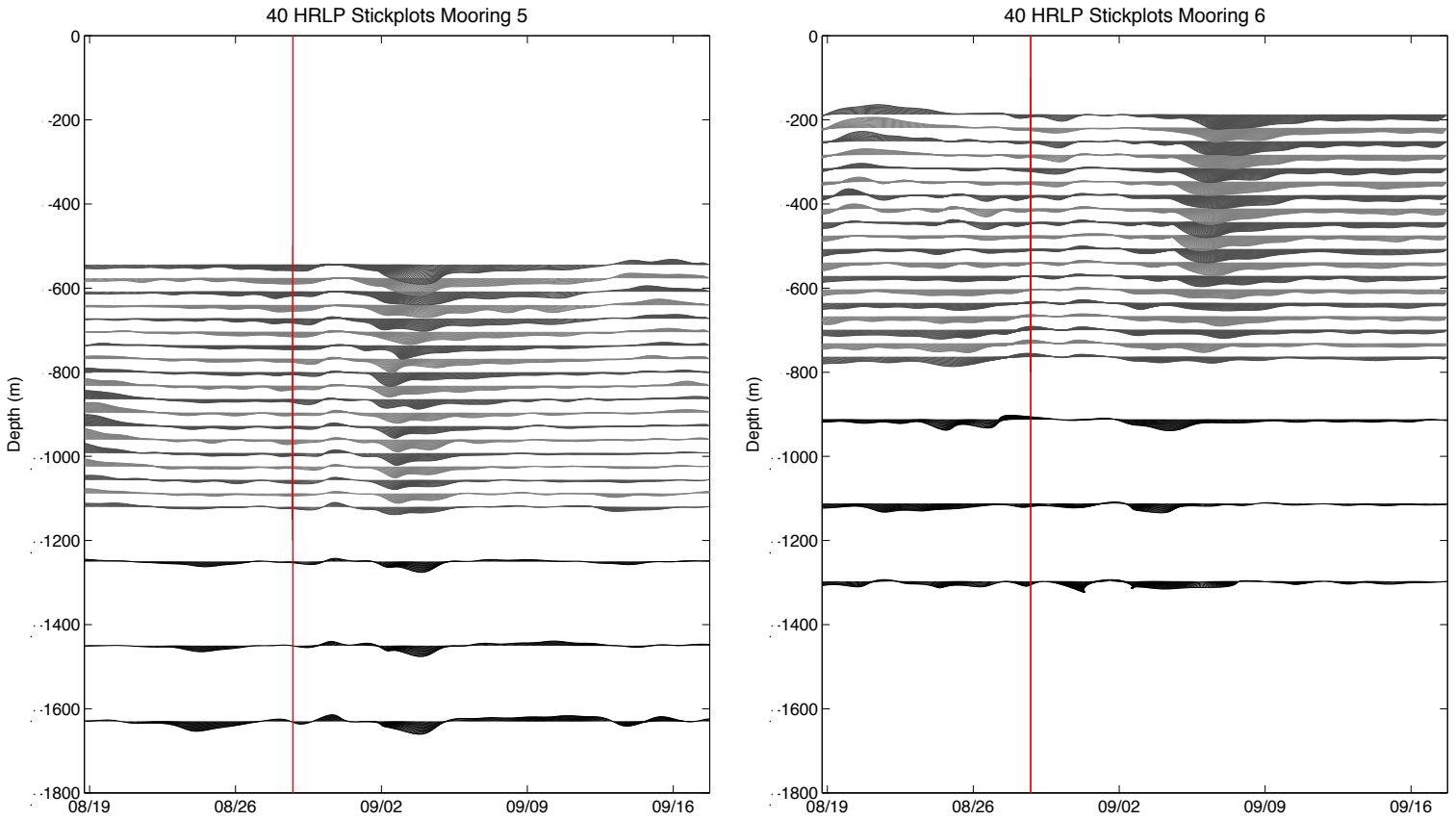


Figure 13 continued.

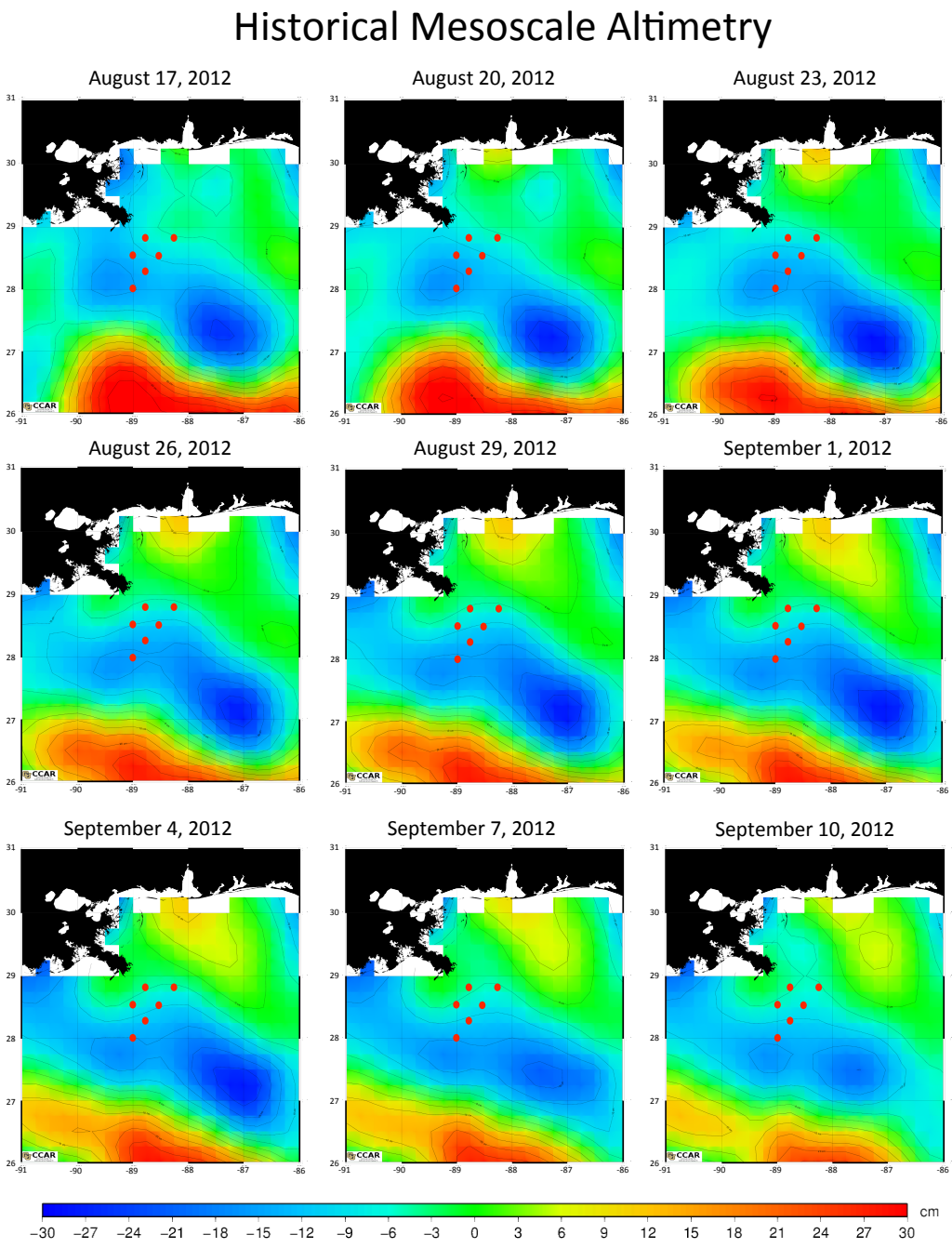


Figure 14. Historical Mesoscale Altimetry during Hurricane Isaac. The center figure (August 29, 2012) corresponds to the closest approach of the hurricane. Altimetry figures show the estimated sea surface height in cm for the region between 26N and 31N and 91W and 86W. Red dots indicate the location of the moorings. Red (blue) colors correspond to positive (negative) sea surface heights indicating anti-cyclonic (cyclonic) rotation. Source: http://eddy.colorado.edu/ccar/data_viewer/index.

The pre-storm hydrographic conditions are determined from CTD casts collected on the G01 mooring deployment cruise in early July 2012 approximately 2 months before the storm. These casts show the temperature and salinity relationships in the area of the moorings as shown in Figure 7. The thermocline thickness and mixed layer thickness is approximately 400 m and 50 m respectively based on the density and temperature profiles of each cast (not shown). Brunt–Väisälä frequency profiles calculated from the CTD casts at each mooring location before deployment are shown in Figure 15. An average Brunt–Väisälä frequency profile, $N^2$, is obtained from casts taken near the mooring locations. This average profile will be used when estimating group velocities of near-inertial internal waves observed after the hurricane. The profile indicates relatively strong stratification in the upper part of the water column above 200 m compared to the rest of the water column. Larger scales of $N$ correspond to stronger vertical density gradients in the water column.

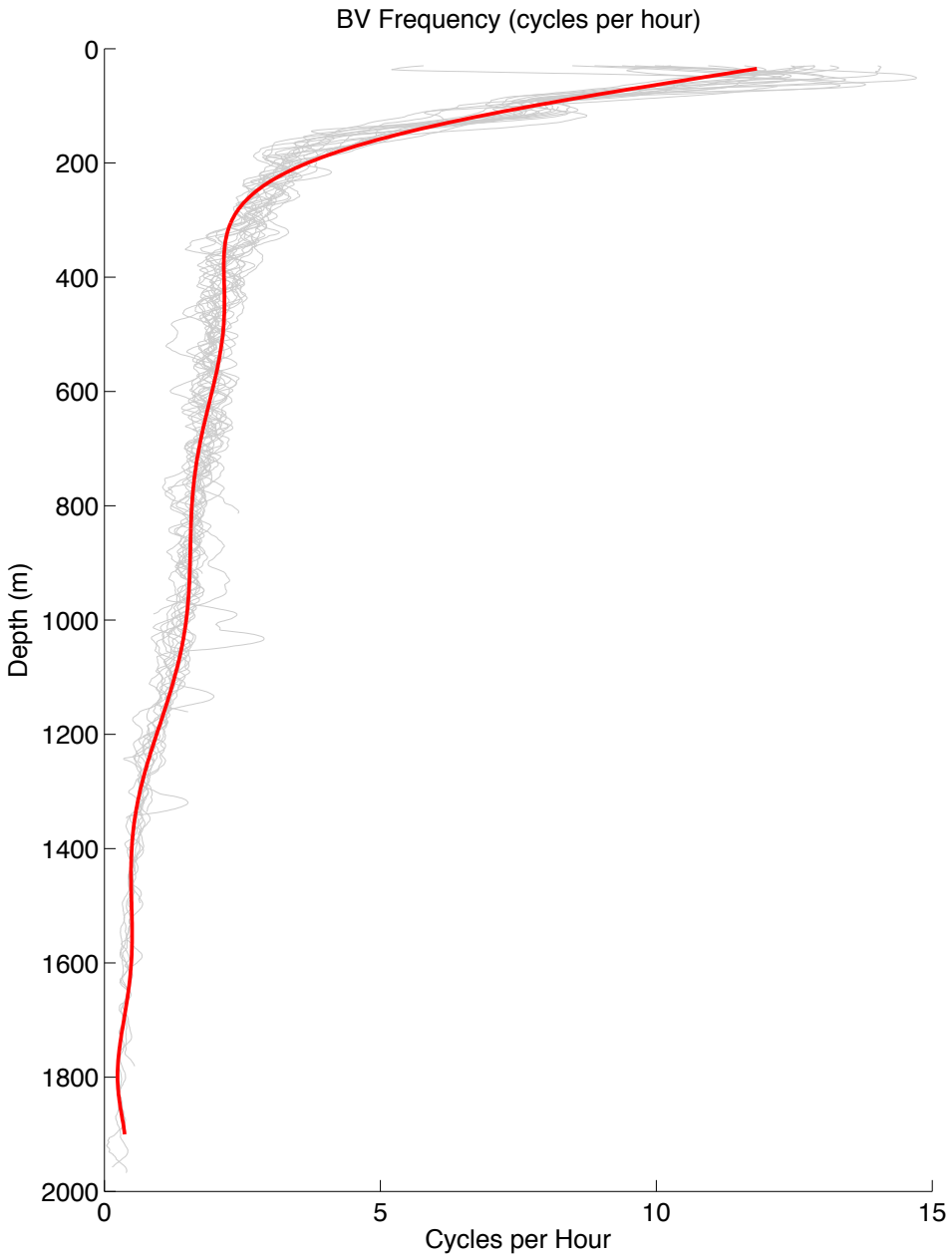


Figure 15. Brunt–Väisälä frequency Profiles. Brunt–Väisälä frequency profiles from CTD casts taken during the G01 mooring deployment cruise in July 2012. The gray lines represent each individual mooring's Brunt–Väisälä frequency profile, and the red line is the estimated best-fit profile used for calculations.

### 3.1.3 Relative Vorticity

Relative vorticity time series calculated from the 40 HRLP records on each side of the storm track are shown in Figure 16. Recall negative relative vorticity corresponds to anticyclonic circulation and positive relative vorticity corresponds to cyclonic circulation. On the right side of the storm track (Moorings 1, 2 and 3), the observed relative vorticity is strongly negative before the storm, which corresponds to anticyclonic circulation. On the left side of the storm track, calculated using velocity data from Moorings 1, 4 and 6, the relative vorticity is positive, corresponding to cyclonic circulation, before the approach of Hurricane Isaac. On the right side of the hurricane track, the relative vorticity is negative before the storm (approximately -.1), and then strongly increases with the passing of the cyclonic storm (from -.15 to -.05 within one inertial period). The relative vorticity then changes to positive approximately 5 days after the storm. The relative vorticity on the left side of the hurricane was positive (approximately .05) before the storm's approach. The relative vorticity remained positive for approximately one day after the passage of the storm before decreasing to negative relative vorticity one day later. The relative vorticity on the left side remained negative for about 5 - 7 days before returning to positive vorticity. The right side of the storm experiences the greatest change in relative vorticity as a result of Hurricane Isaac (from -.015 to -.05). This is consistent with the expectation of an asymmetrical current response to Hurricane Isaac with greater currents observed on the right side of the storm track.

The gradients of relative vorticity on the right side of the hurricane track tighten in response to the Hurricane as observed in top plot of Figure 17. Figure 17 shows the contour plots of the relative vorticity, normalized by the local Coriolis frequency, f, on each side of the storm track. The color scales are the same for each figure, showing the higher values of relative vorticity and tighter gradients observed on the right side of the Hurricane track compared to the left side.

### 3.1.4 Wind Stress/Wind Curl

The wind stress and wind stress curl for the time period near Hurricane Isaac were estimated from model wind output as described in Section 2.1.4. The strong cyclonic signature of the hurricane is observed in the extreme wind stress vector values shown in the left column of Figure 18. The wind stress curl was near zero before the storm and became positive as the hurricane approached before turning negative after the passing of the storm. The right side of the storm track experienced the greatest magnitude of wind stress curl due to Hurricane Isaac, while the left side of the storm track experienced the smallest magnitude of wind stress curl as a result of Hurricane Isaac's passage. The estimate of wind stress near the moorings is used to determine descriptive parameters for Hurricane Isaac. These wind stress vectors confirm that the cyclonic wind stress curl from Hurricane Isaac likely caused the strong cyclonic current response observed in the current meter data.

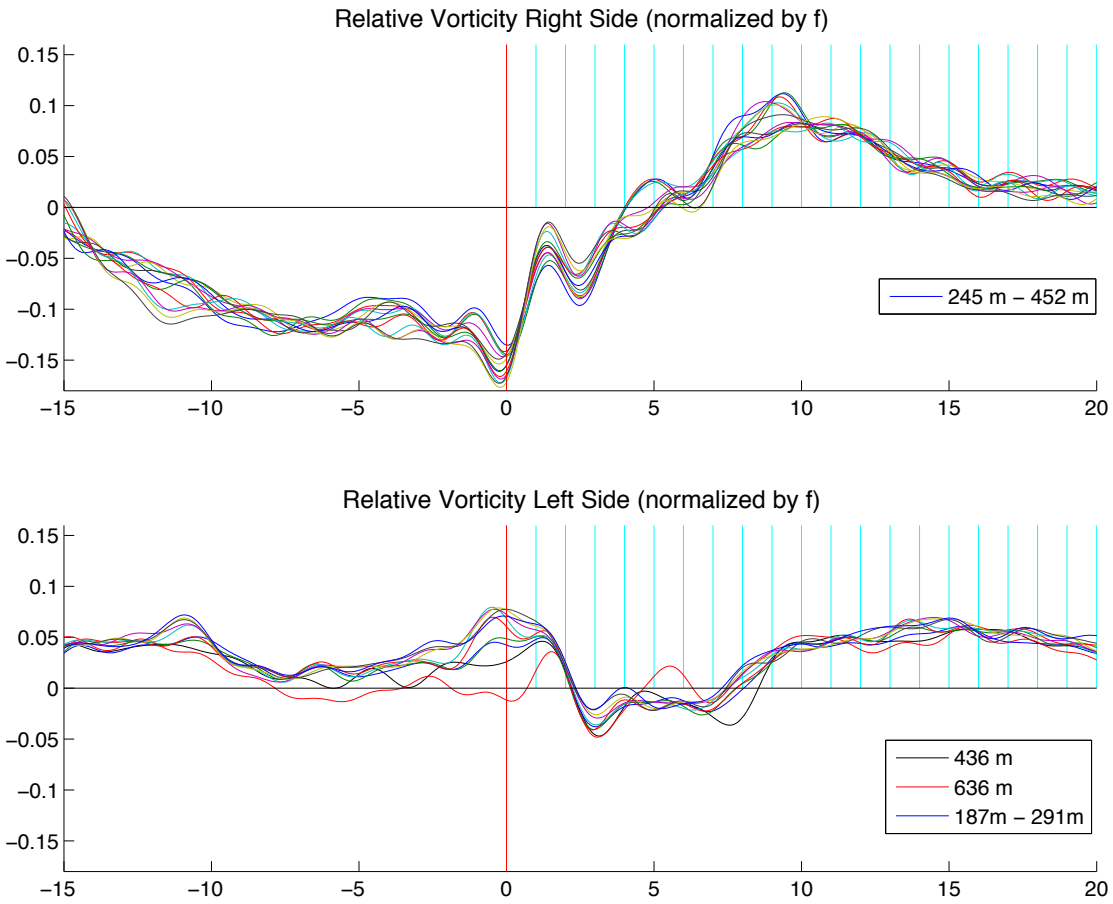


Figure 16. Relative Vorticity Time Series. Relative vorticity normalized by f on the left and right sides of the Hurricane Isaac storm track between -15 inertial periods and 20 inertial periods. The red vertical line represents the closest approach of Hurricane Isaac. The right side relative vorticity is estimated from ADCP time series records between 245 and 452 m at Moorings 1, 2 and 3. The left side relative vorticity is estimated from ADCP time series records between 187 and 291 m and RCM records at 436 m and 636 m at Moorings 1, 4, and 6.

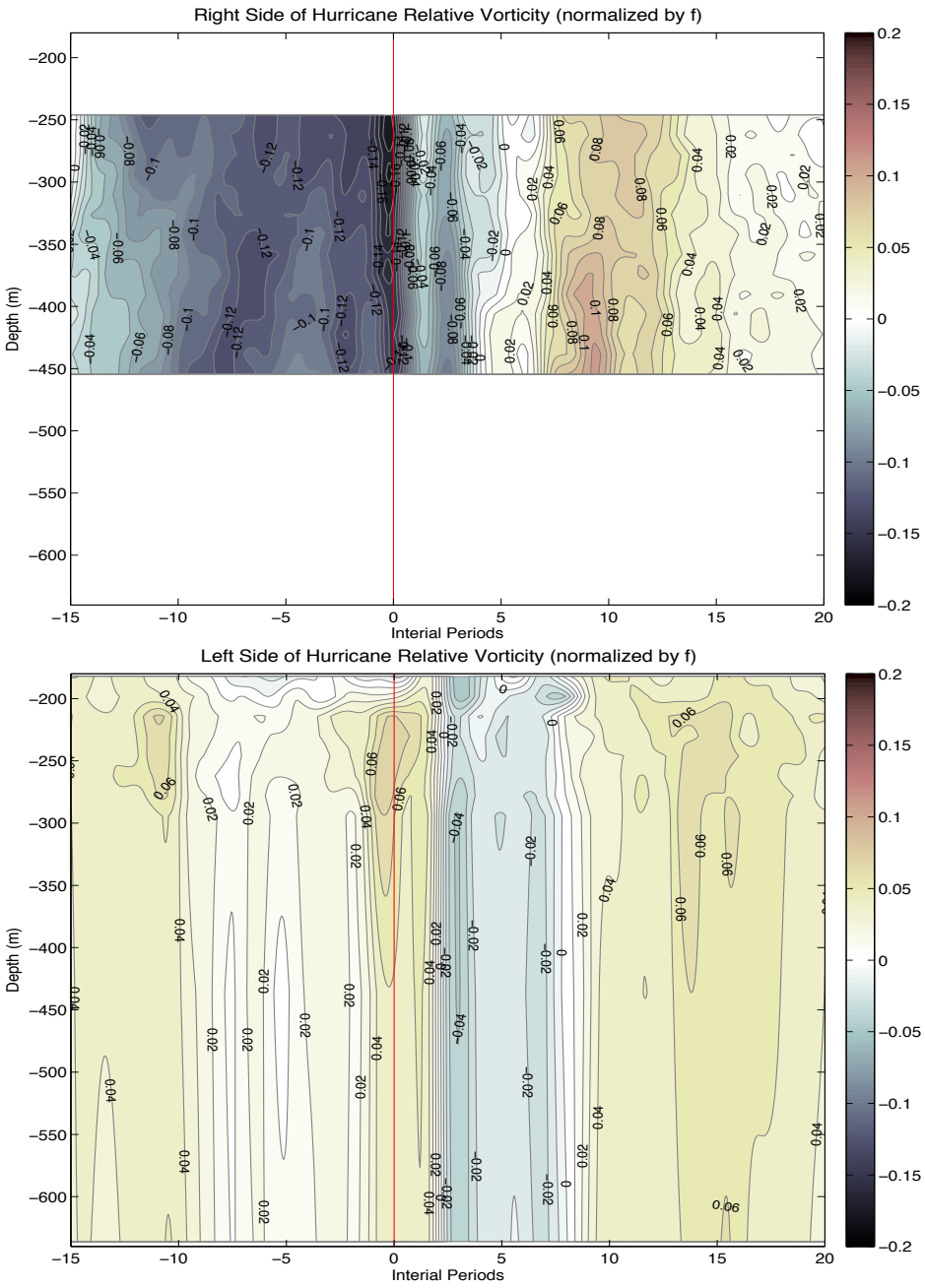


Figure 17. Relative Vorticity Contours. Relative vorticity contours normalized by f on the left and right sides of the Hurricane Isaac storm track between -15 inertial periods and 20 inertial periods. The red vertical line represents the closest approach of Hurricane Isaac. The right side relative vorticity is estimated from ADCP time series records between 245 and 452 m at Moorings 1, 2 and 3. The left side relative vorticity is estimated from ADCP time series records between 187 and 291 m and RCM records at 436 m and 636 m at Moorings 1, 4, and 6.

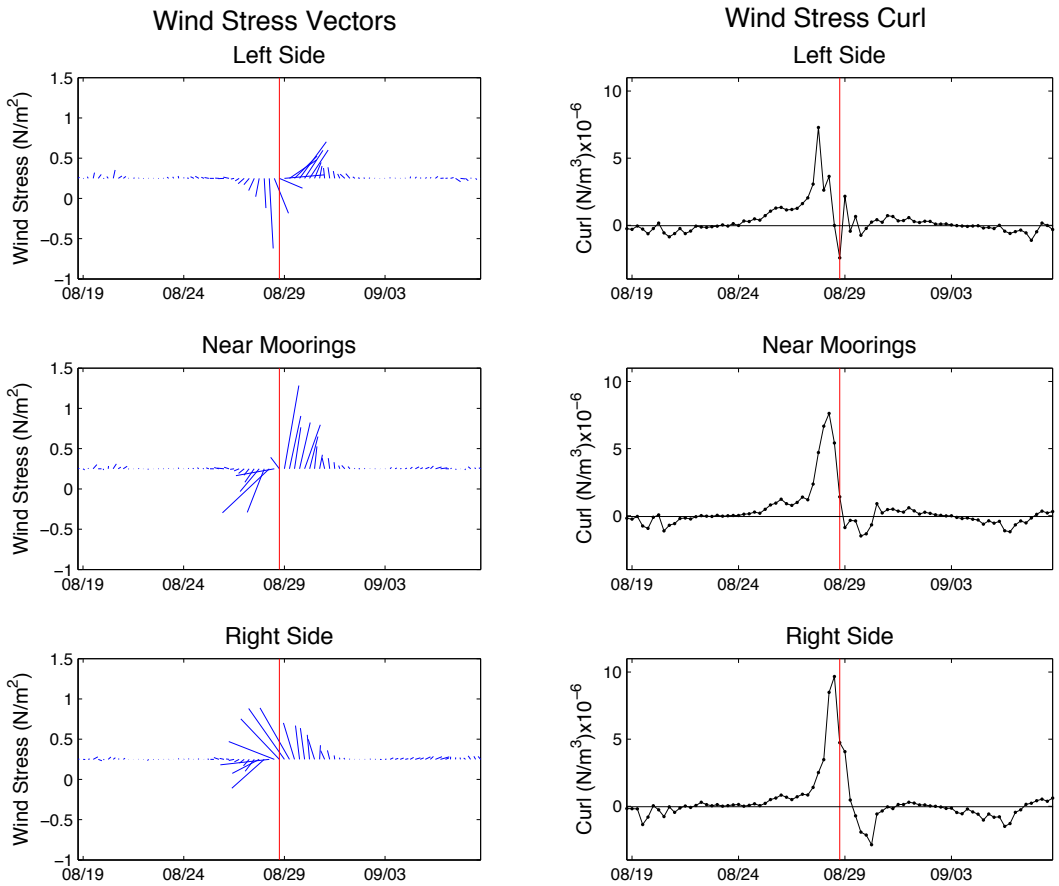


Figure 18. Wind Stress and Wind Stress Curl. Wind stress vectors and wind stress curl time series for sites near the mooring array, to the left of the storm track, and to the right of the storm track as shown in Figure 8. The blue lines in the plots in the left column represent the direction and speed of the wind near the time of Hurricane Isaac, with vertical lines corresponding to north and south, and horizontal lines corresponding to east and west directions. In the right column of plots, each window shows the wind stress curl at each location. The red vertical line indicated the passage of Hurricane Isaac. Dates are in UTC.

### 3.2 Current Extremes

Hurricane Isaac approached the mooring array on late on 28 August 2012, with the eye of the storm passing directly over the mooring array at 18:00 UTC. The currents at each mooring show a strong response to the passing of the Hurricane Isaac in the 40 HRLP velocity vectors in Figure 13.

Before the approach of Hurricane Isaac, Moorings 1, 2, and 3 were flowing generally to the west, northeast, and south respectively. As the hurricane approached, the flow changed to strongly southwestward at each mooring. The maximum current speeds associated with Hurricane Isaac were observed at the shallowest recorded depths within 24 hours of the storm's closest approach to the mooring array. The maximum current speed profiles for each mooring are shown in Figure 19. The top section of each plot shows the maximum recorded current speeds for each depth recorded by the ADCP for the entire year-long record (dashed line), for the passage of the storm (thick line), and the wake of the storm defined as the period of time from 1 day to 14 days after the storm's closest approach to the mooring array on 28 September 2012 (bold line). The bottom section of each plot shows the maximum current speeds for each depth measured in the lower water column using the same identifying lines. Points are also included in the bottom section to show the depths of each measurement. Mooring 1 had the most observations in the lower water column with a total of 6 instruments deployed below the ADCP, while Mooring 2 lacked any lower water column measurements due to the loss of instruments during recovery. The remaining moorings each featured 3 recording current meters (RCMs) that captured the lower water-column response.

Mooring 1, the mooring located nearest to the storm track, observed a maximum current speed of 50 cm/s at the shallowest recorded depth of 86 m within 24 hours of the storm's closest approach. With the exception of Mooring 1 and the near-surface records (above 100 m), the maximum current speeds associated with Hurricane Isaac were observed days later in the storm's wake, not during the passage of the storm. All moorings also observed stronger near-bottom currents speeds during the wake of Hurricane Isaac compared to when the storm passed over the mooring. Figure 19 shows that the near-bottom speeds recorded during the wake of Hurricane Isaac were the maximum speeds observed during the yearlong records, but at all other depths the maximum current speeds were not observed during the passage or the wake of Hurricane Isaac.

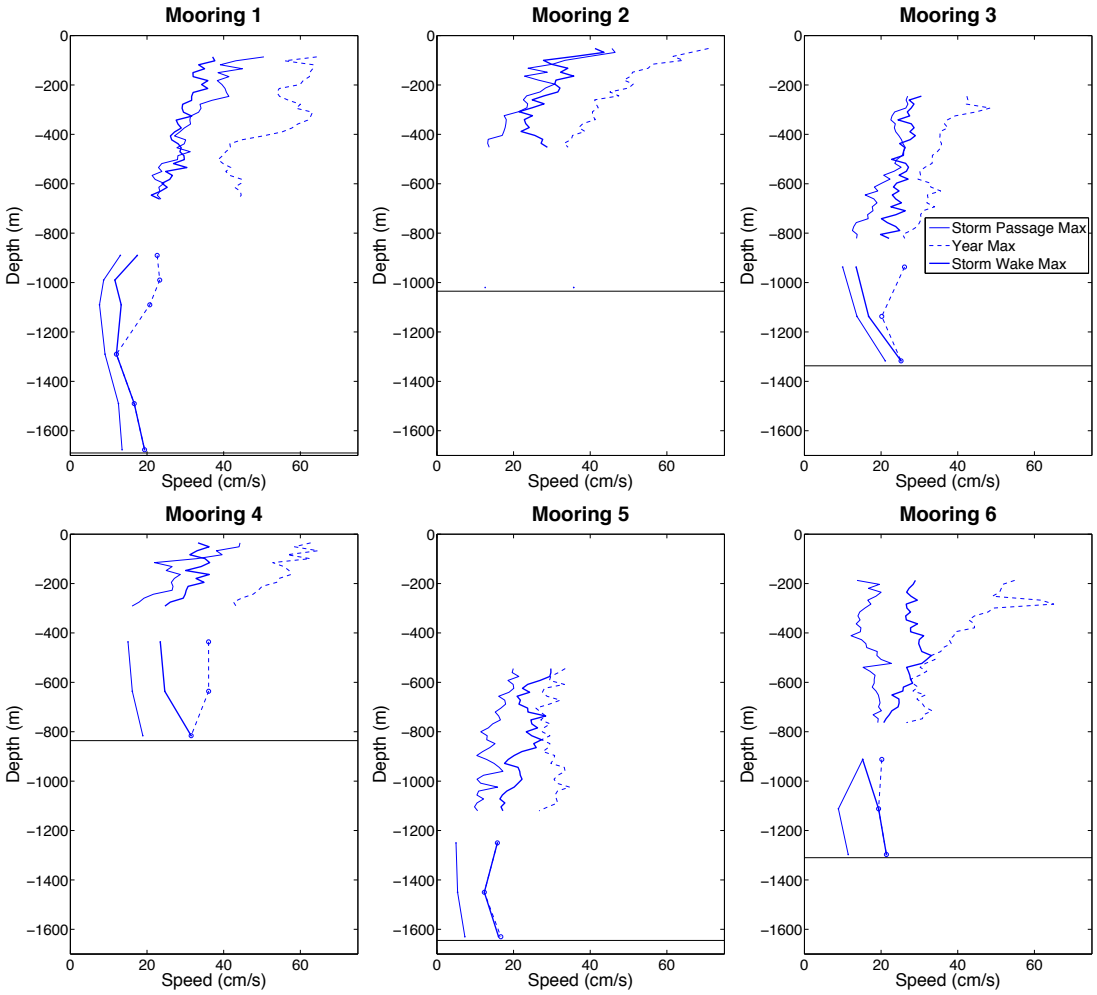


Figure 19. Maximum Current Speed Profiles. Maximum current speeds for Hurricane Isaac during the period of the storm (thin straight line), in the wake of the storm (bold straight line), and for the yearlong time series (dashed line). The top section of each plot shows the ADCP data and the bottom section shows the RCM and S4A data, all at their corresponding depths. The statistics were calculated from the quality controlled unfiltered velocity data. The storm wake refers to the period 1 to 14 days after the time of the storm's closest approach to the mooring array at 18:00 UTC 28 August, 2012.

### 3.3 Near Inertial and Sub-inertial Response

In addition to high currents speeds observed during the wake of Hurricane Isaac, a strong near-inertial oscillation and two sub-inertial oscillations with periods of 2-5 days and 5-12 days are observed in each of the mooring velocity records using spectral analysis (Figure 20) and wavelet analysis. Figure 9b shows a clear increase in power (variance) near the 1-day period, between 2 and 5 days, then again between 5 and 12 days. All moorings showed a strong increase in variance in the near inertial band in the upper water column, but not all moorings experienced the same degree of variance in each sub inertial band. Spectra for the u and v velocity components for Moorings 2 and 4 in Figure 20 show a noticeable peak in variance in the range of periods between 2 and 5 days. The variance is generally larger for shallower depth levels at each mooring. Table 3 shows the depth averaged variance percentages for the year record and the Hurricane Isaac period for each velocity component from each ADCP in the near inertial band, the first sub-inertial band and the second sub-inertial band respectively. The moorings located nearest the storm track (M1, M2 and M4) experienced the maximum increase in variance in the near inertial band at shallower depths (less than 150 m). Moorings 3, 5, and 6 all experienced maximum increases in variance associated with the near inertial band much deeper in the water column (between 700 and 900 m).

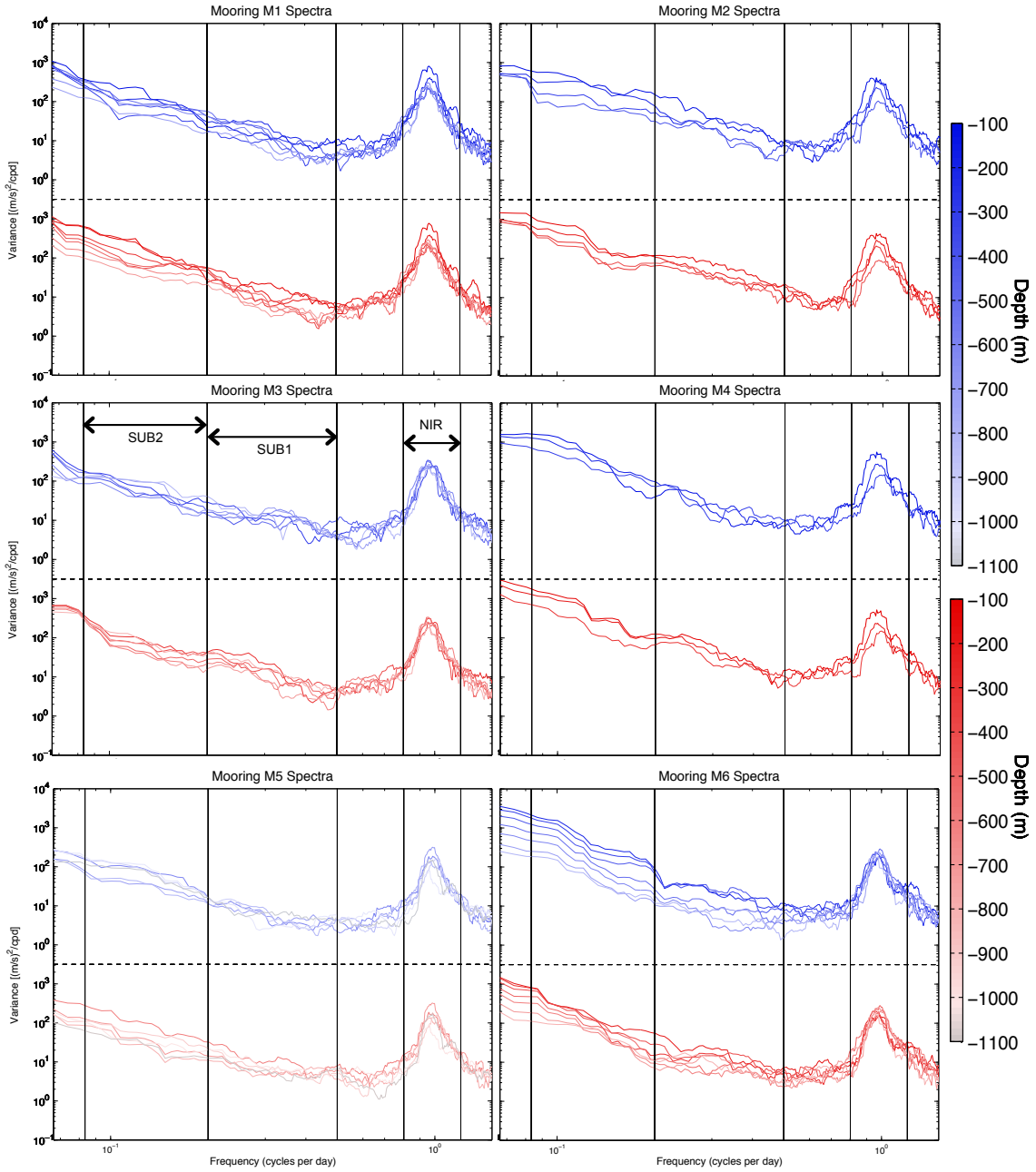


Figure 20. Spectra for ADCP data. Spectra for velocity components u (red) and v (blue) for each 100m-depth level available from each ADCP. Darker colors correspond to shallower depths. Black vertical lines in each figure correspond to frequency intervals (NIR band: .8f-1.2f, SUB1 band: 2-5 days, and SUB2 band: 5-12 days). Velocity records were analyzed for the time interval from 42 days before the storm and 85 days after the storm.

| NIR Band | | | | | |
|---|---|---|---|---|---|
| Mooring | Velocity Component | Depth Avg Variance % Year | Depth Avg Variance % Storm | Max Variance % Storm | Max Variance % Depth (m) |
| 1 | *u* | 9.1 | 26.9 | 58.8 | 86.2 |
| | *v* | 17.3 | 18.5 | 44.6 | 86.2 |
| 2 | *u* | 7.2 | 22.1 | 47.3 | 84.2 |
| | *v* | 10.1 | 25.4 | 54.5 | 68.2 |
| 3 | *u* | 11.1 | 36.4 | 53.1 | 741.2 |
| | *v* | 16.4 | 21.5 | 46.5 | 757.2 |
| 4 | *u* | 9.9 | 26.5 | 49.5 | 67.2 |
| | *v* | 11.6 | 32.3 | 75.1 | 67.2 |
| 5 | *u* | 23.3 | 33.1 | 55.4 | 848.2 |
| | *v* | 23.0 | 24.5 | 35.9 | 848.2 |
| 6 | *u* | 15.2 | 22.4 | 38.5 | 699.2 |
| | *v* | 13.9 | 25.7 | 45.2 | 699.2 |

| SUB1 Band | | | | | |
|---|---|---|---|---|---|
| Mooring | Velocity Component | Depth Avg Variance % Year | Depth Avg Variance % Storm | Max Variance % Storm | Max Variance % Depth (m) |
| 1 | *u* | 1.1 | 3.1 | 6.4 | 150.2 |
| | *v* | 3.0 | 4.0 | 6.8 | 214.2 |
| 2 | *u* | 3.0 | 17.7 | 28.0 | 132.2 |
| | *v* | 4.0 | 7.3 | 15.9 | 116.2 |
| 3 | *u* | 1.8 | 5.1 | 8.1 | 357.2 |
| | *v* | 3.0 | 2.2 | 3.7 | 629.2 |
| 4 | *u* | 2.8 | 7.0 | 11.0 | 259.2 |
| | *v* | 2.9 | 7.3 | 11.7 | 147.2 |
| 5 | *u* | 2.0 | 6.3 | 9.9 | 768.2 |
| | *v* | 2.1 | 4.1 | 7.3 | 976.2 |
| 6 | *u* | 1.8 | 4.6 | 9.4 | 763.2 |
| | *v* | 1.4 | 5.9 | 14.1 | 395.2 |

Table 3. ADCP Variance Table. Tables of depth averaged variance percentages for each ADCP velocity component data for the yearlong record and the Hurricane Isaac storm period. The storm period variance was calculated for velocity records between August 18, 2012 and September 12, 2012.

| SUB2 Band | | | | | |
|---|---|---|---|---|---|
| Mooring | Velocity Component | Depth Avg Variance % Year | Depth Avg Variance % Storm | Max Variance % Storm | Max Variance % Depth (m) |
| 1 | *u* | 4.3 | 10.0 | 17.5 | 214.2 |
| | *v* | 7.4 | 9.6 | 12.8 | 614.2 |
| 2 | *u* | 6.6 | 8.0 | 19.2 | 52.2 |
| | *v* | 8.0 | 7.4 | 11.1 | 132.2 |
| 3 | *u* | 5.8 | 3.4 | 5.3 | 453.2 |
| | *v* | 12.0 | 3.8 | 7.8 | 821.2 |
| 4 | *u* | 6.5 | 18.5 | 26.9 | 195.2 |
| | *v* | 8.4 | 21.3 | 31.5 | 179.2 |
| 5 | *u* | 4.9 | 6.1 | 13.8 | 928.2 |
| | *v* | 5.0 | 14.1 | 19.6 | 1104.2 |
| 6 | *u* | 4.8 | 14.1 | 26.5 | 747.2 |
| | *v* | 5.3 | 10.1 | 15.3 | 747.2 |

Table 3 continued.

The variance associated with the SUB1 and SUB2 bands consistently increased during the storm at all moorings except Mooring 3 in SUB2 band. Moorings 2 observed the greatest increase in variance associated with the SUB1 band, over 25% of the total variance in the u velocity component, while the other moorings experienced only small increases in variance (15% or less of total variance during the storm period). The SUB2 band observed consistently greater percentages of variance associated with the passage of Hurricane Isaac with the exception of Mooring 3. Mooring 3 actually experienced a decrease in variance (40-70% decrease) associated with the SUB2 band during the period of the storm. Mooring 4 observed the greatest amount in variance (over 25%) in both the u and v velocity components associated with the SUB2 band between 150 and 200 m. Mooring 6 also observed higher amounts of variance in u velocity component

variance percentage (over 25%) near 800 m associated with the SUB2 band. Mooring 2 observed a high amount of variance of nearly 20% above 100 m in the u velocity component record associated with the SUB2 band.

### 3.3.1 Near Inertial Response

A wake of near inertial internal waves was observed at all moorings after Hurricane Isaac passed over the GISR mooring array on 28 August 2012. The strong near inertial oscillations are observed immediately after the passage of the storm and persist for approximately 10-15 days (Figure 21). The propagation of near-inertial energy into the water column is apparent in Moorings 1, 3 and 4 while near-inertial energy is trapped near the surface at Mooring 2. Wavelet analysis performed on the current meter records revealed an increase in the effective frequency of the near inertial band after the passage of Hurricane Isaac. An increase in the near inertial band frequency was observed in the band pass filtered velocity records from all moorings. The frequency shift began approximately 2 inertial periods after the storm and lasted for about 5 inertial periods. Wavelet analysis was performed on the current meter records captured by the ADCP at Mooring 1, and then the resulting output was partitioned between 2 and 7 inertial periods after the storm to isolate the storm's wake and highlight the shift in frequency. Figure 22 shows the frequency shift observed at Mooring 1 from 2-7 inertial periods after the storm at every other ADCP depth level using a product of wavelet analysis. Each partition was plotted below the previous depth level in order to show how the inertial frequency changed throughout the water column in the wake of the storm. Warmer colors (reds) represent greater variance, while the cooler colors

(blues) represent less variance. The strongest amounts of variance are observed higher in the water column at 118 m as seen in Figure 22. Also, there is a shift of the highest level of variance to a lower period (higher frequency) in the wake of Hurricane Isaac. The analysis shows that this observed near inertial frequency was generally less than the local Coriolis frequency at each mooring location, indicating a "blue shift" in frequency. The average effective frequency observed at each mooring was 1.11$f$ with $f$ being the local Coriolis frequency. A similar blue shift in frequency was observed in response to Hurricane Isaac at all other moorings.

3.3.1.1 Phase Shift

The deployment depths of each mooring limited the amount of velocity data available from the upper water column. Only Moorings 1, 2 and 4 measured velocity data above 100 m with the shallowest recorded depths being 86 m at Mooring 1, 52 m at Mooring 2, and 35 m at Mooring 4. At Moorings 2 and 4, there was a phase difference observed between the mixed layer and the upper thermocline where leading phases with increasing depth are observed in Figure 21. Mooring 2 had near inertial energy trapped in the mixed layer, above 100 m. The depth of near inertial energy at Mooring 4 was initially be much deeper in the water column, ~150 m, and a depth-leading phase appears within 2 inertial periods after the passage of Hurricane Isaac. Mooring 1 also experienced a depth-leading phase with higher amplitudes beginning after 2 inertial periods of the storm's passage. Moorings 1 and 3 showed coherent vertical phase distributions profiles, with a gradual decrease in phase with increasing depth (3 hours phase lead at 198 m compared to 86 m at Mooring 1).

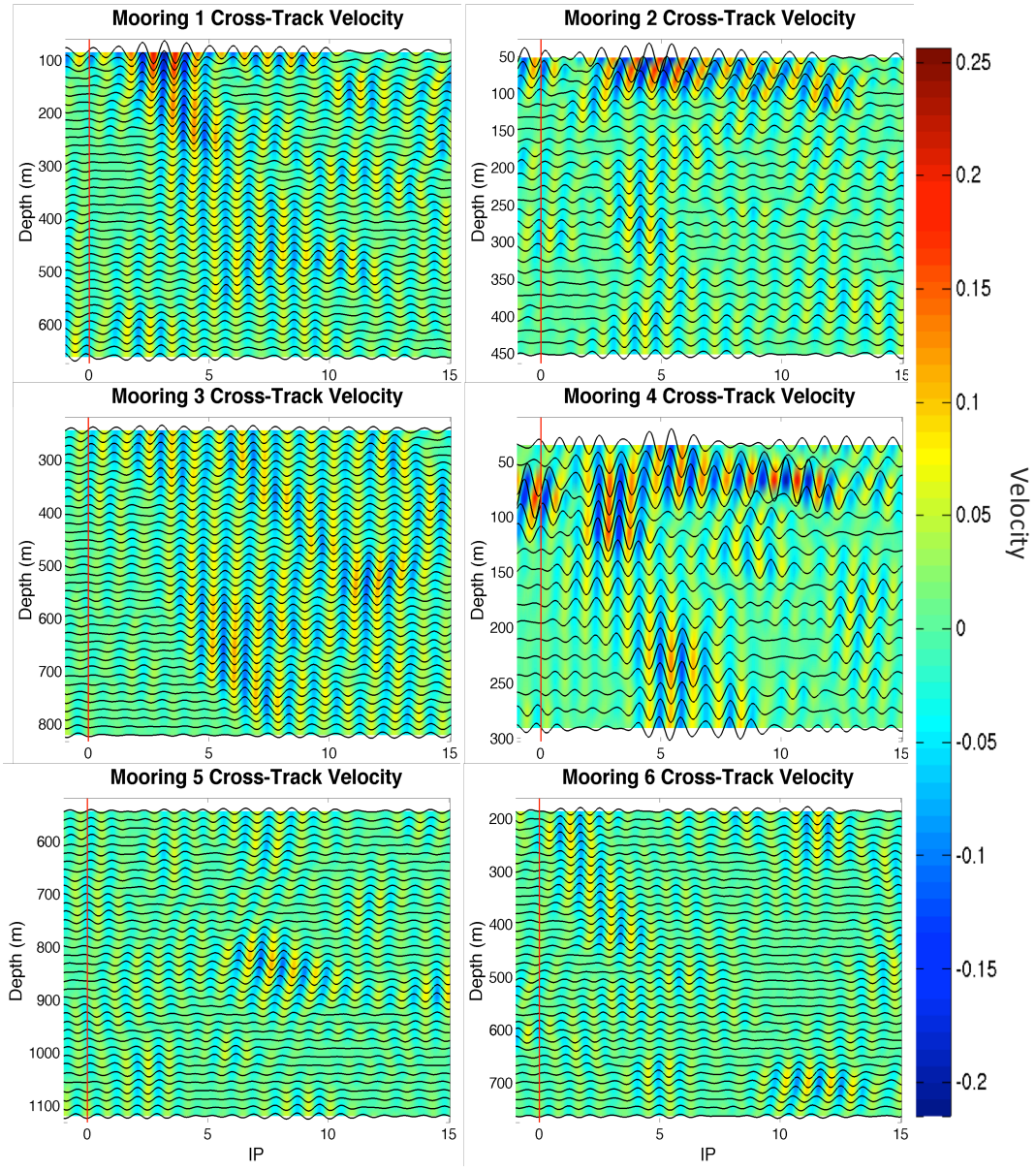


Figure 21. Hovmöller Diagrams for NIR currents. Hovmöller Diagrams of the cross track component of velocity measured from ADCP at each mooring location from one inertial period before the storm to 15 inertial periods after the storm. The red vertical line refers to the time of the closest approach of Hurricane Isaac. The background color in each plot refers to the amplitude of the measured velocity in m/s. The near inertial band-passed record for each available depth from the ADCP is overlaid at the corresponding depth as a black line. Notice that the depth ranges of each figure vary according to the depth of the ADCP.

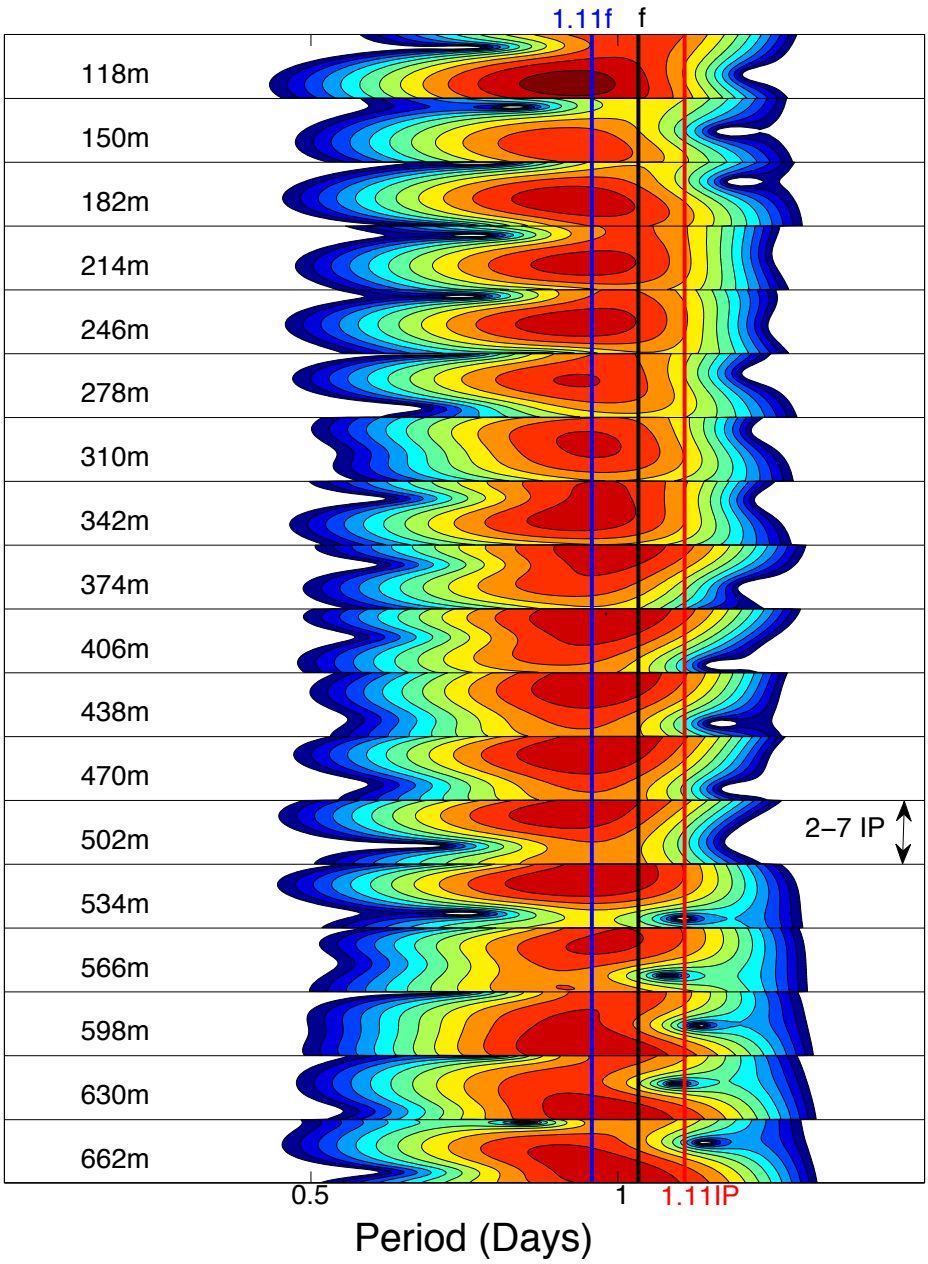


Figure 22. Frequency Shift at Mooring 1. Mooring 1 near-inertial partitioned wavelets at depths captured by the ADCP show the blue shift in frequency in the wake of Hurricane Isaac. Each slice represents the 2-7 inertial period partition of the wavelet of the current meter record from the each depth. The black line is the local inertial period, or local Coriolis frequency *f*, at Mooring 1. The blue line is 1.11*f*, representing the average blue shift in frequency observed in the wake of the storm. The red line represents 1.11 IP, or .9*f*, which would be a red shift in frequency. Warmer colors represent higher variance observed at the corresponding period.

This positive tilt in the phase distribution with depth is indicative of downward propagation of energy into the thermocline.

Comparison between similar depth levels between moorings using wavelet coherence analysis confirms the propagation direction of the near-inertial energy was away from the storm path. Figure 10 shows the wavelet coherence between the 600 m depth records at Mooring 1 and Mooring 3. Mooring 1 and Mooring 3 are aligned perpendicular to the storm track with Mooring 1 being closest to the storm path. The direction of the phase arrows in the wavelet coherence analysis (Figure 10) shows that the two records are strongly coherent and nearly in phase in the near-inertial band, with the phase of Mooring 3 leading Mooring 1. This small phase lead indicates propagation of near-inertial energy from Mooring 1 to Mooring 3, or away from the storm track.

3.3.1.2 Vertical Scale

The phase difference of 3 hours between the shallowest depth at Mooring 1 (86 m) and the thermocline (198 m) indicates a vertical scale of approximately 845 m after 3 inertial periods following the storm. This is larger than the thermocline thickness, but smaller than the total water depth. After 5 inertial periods after the storm, the phase lead with depth increased to 4 hours, indicating a new vertical scale of 633 m.

A phase difference of one hour was observed between the mixed layer at Mooring 4 (35 m) and the upper thermocline (86 m) just 3 inertial periods past the storm's passage. This indicated a vertical scale of approximately 1086 m. The phase difference increased to a 3-hour phase lead in the upper thermocline 5 inertial periods after the storm, indicating a much smaller vertical scale of 362 m. The estimated vertical

scale for the near-inertial response will be 965 m, the average of the Mooring 1 and Mooring 4 vertical scales. The vertical wavenumber for the near-inertial response will be 0.03 $km^{-1}$.

Between 4 and 5 inertial periods after the storm, both Mooring 1 and Mooring 4 experience an amplitude minimum in the depths between 100 and 200 m. The maximum phase difference measured between the mixed layer (52 m) and the upper thermocline (100m) at Mooring 2 was 9 hours, indicating a vertical scale of only 120 m. At Mooring 2, the near inertial energy was trapped in the mixed layer and unable to penetrate into the thermocline.

3.3.1.3 Horizontal Scale

A horizontal cross-track scale of 176 km to 235 km was calculated from the observed phase difference of 3 to 4 hours between the rotated u-velocity records at Mooring 1 and Mooring 3 near 300 m. The 176 km horizontal along-track scale was calculated at the same time period from the phase differences of 4 hours between the rotated v-velocity records at Moorings 1 and 2 at 200 m. The estimated horizontal scale for the near-inertial response will be 205 km, the average of the scale determined between Mooring 1 and Mooring 3 and between Mooring 1 and Mooring 2. The horizontal wavenumber for the near-inertial response will be 6.6 $km^{-1}$.

The phase angle calculated from the spatial scales is $\tan \theta = 0.004$ (.27 degrees), compared with the $\tan \theta = 0.007$ (.44 degrees) estimation from the dispersion relation. The estimated horizontal and vertical group velocities were calculated using the average vertical and horizontal wavenumbers (l, m) = (0.03 $km^{-1}$, 6.61 $km^{-1}$) and the estimated

Brunt–Väisälä frequency of 3.7 cycles/hr. The horizontal group velocity ($C_{gy}$) was approximately 5.7 km/day and the vertical group velocity ($C_{gz}$) was approximately 29 m/day into the water column calculated from Equations 5a and 5b (Brooks 1983)..

The downward propagation of energy in the near-inertial band is also observed in the wavelet analysis of the current meter records from the ADCPs. Figure 23 shows the scale average of variance of the north-south velocity component at each depth for each ADCP location. The scale average of variance for each time series is a vertical integration of the wavelet power spectrum of the periods between 12 and 36 hours (as in Figure 9d). The integrated values are obtained for each depth level to show the time and space evolution of variance within the NIR (near-inertial) band at each mooring. Figure 23 shows the confinement of near-inertial energy in the mixed layer at Mooring 2 and the propagation of energy into the thermocline at Mooring 1 and Mooring 3. The color scales are independent between each mooring in order to better show the propagation of energy into the water column.

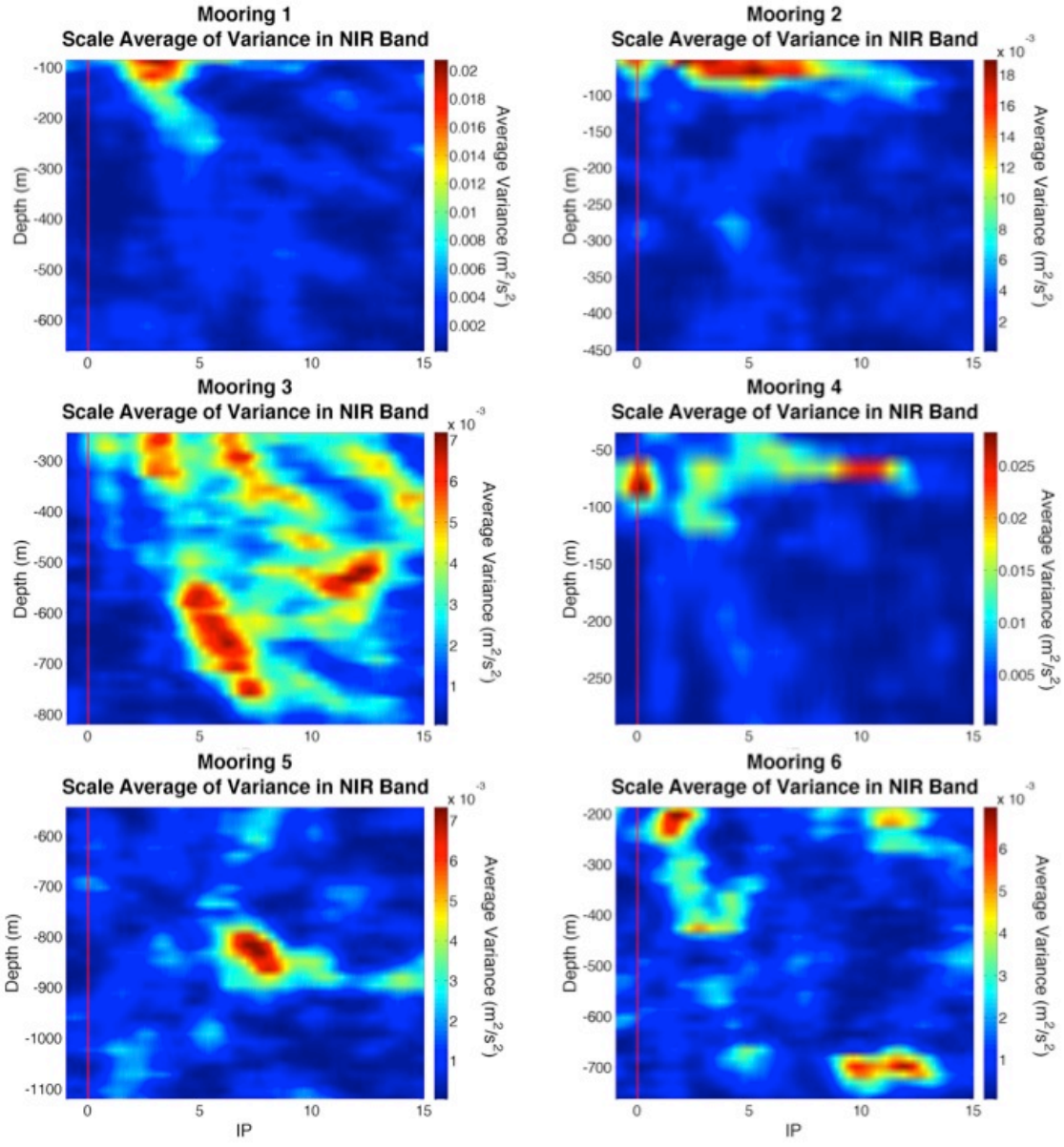


Figure 23. Scale Average of Variance in the NIR Band. Scale average of variance in the north-south velocity component measured from the ADCP at each mooring location from one inertial period before the storm to 15 inertial periods after the storm. The red vertical line refers to the time of the closest approach of Hurricane Isaac. The background color in each plot refers to the amount of variance measured at the corresponding time and depth level. The color scales are independent for each mooring.

### 3.3.2 Sub-Inertial Response

In addition to the strong near-inertial response in the wake of Hurricane Isaac, two distinct sub-inertial period waves were observed in the current meter records. One sub-inertial wave is characterized by a 2-5 day period (0.5-0.2 cpd frequency) and featured maximum speeds associated with this band of over 16 cm/s. This sub-inertial band will also be referred to as the SUB1 band. The second sub-inertial wave had a longer period between 5 and 12 days (0.08 – 0.2 cpd frequency) and expressed a smaller degree of speed, 12.5 cm/s maximum at Mooring 4, but accounted for a higher percentage of the total variance observed in the current meter records as seen in Table 3. This band will also be referred to as the SUB2 band. The current responses at all moorings and in each sub-inertial band show a strong barotropic response that is observed throughout the water column and varies in intensity between each mooring. Barotropic flow is defined as a geostrophic flow with no vertical sheer and is driven only by horizontal variation in sea surface height (Talley et al. 2011). This strong barotropic response is fundamentally different than the near-inertial response. The sub-inertial response is simultaneous throughout the water column, whereas the near-inertial response propagates downward through the water column.

Horizontal wavelengths and propagation speeds for these sub-inertial waves could not be calculated due to the inconsistent observations of these waves between the moorings. Despite the close proximity of the moorings to the storm track, the records did not show coherence phase between moorings. Also, the arrangement of the moorings in the water column did not allow for acceptable reliable estimations of horizontal

speeds. Wavelet coherence analysis on the velocity records show strong coherency (< 0.8) in both sub-inertial bands during the passage of Hurricane Isaac, but no consistent direction of propagation could be determined. The lack of evidence to support propagation of the sub-inertial waves is also consistent with a non-propagating barotropic response. The strong vertical coherence observed between depth levels at each mooring does suggest the sub-inertial responses were forced by the passage of Hurricane Isaac.

3.3.2.1 SUB1

The sub inertial band with a period between 2 and 5 days, SUB1, featured the maximum speeds associated with this band at Mooring 2. The maximum speeds measured 17 cm/s and were observed in the upper 100 m of the water column at Mooring 2. Although Mooring 2 experienced the highest speeds in response Hurricane Isaac, all moorings observed a barotropic response throughout the water column measured by the ADCP as shown in Figure 24. The SUB1 response began before the closest approach of Hurricane Isaac to the mooring array (red vertical line in Figure 24) and last for a total of 3-5 oscillations or approximately 5-7 days after the passage of the storm. Each moorings observed a bottom intensified response in the RCM data collected 20 m above the ocean floor. The full water column profile for each mooring suggests bottom intensification with a gradual decrease in amplitude with decreasing depth. Mooring 4 was the only mooring to observe a strong phase shift between the shallowest record and the deeper current meter records. With the exception of the upper most records of Mooring 4, all velocity profiles observed strong coherency with depth

consistent with a barotropic response in the SUB1 band. A consistent propagation direction for this SUB1 response is unable to be determined.

Moorings 2 and 4 were deployed in shallower water than the other moorings, 1035 m and 836 m respectively, compared to the other moorings that were all deployed below 1300 m. These shallow moorings experienced the maximum current response in the 2-5 day sub-inertial band compared to the deeper moorings. Figure 25 and Figure 26 show the wavelet products of scale average of variance in the 2-5 day sub-inertial response to Hurricane Isaac similar to Figure 23 for the near-inertial band. Figure 25 shows the shallower Moorings 2 and 4 on the same color scale. The remaining moorings deployed in deeper water are shown in Figure 26. The response was much greater at Moorings 2 and 4 compared to the deeper moorings, therefore the color scales differ between Figure 25 and Figure 26. Each figure shows the overlay of the depth anomaly time series derived from the pressure recorded at each ADCP instrument. The depth anomaly records are band passed for the 2-5 day period and plotted at the depth level at which they were recorded. Mooring 2 observed the maximum depth anomaly of over 30 cm associated with the 2-5 day period band in the wake of Hurricane Isaac.

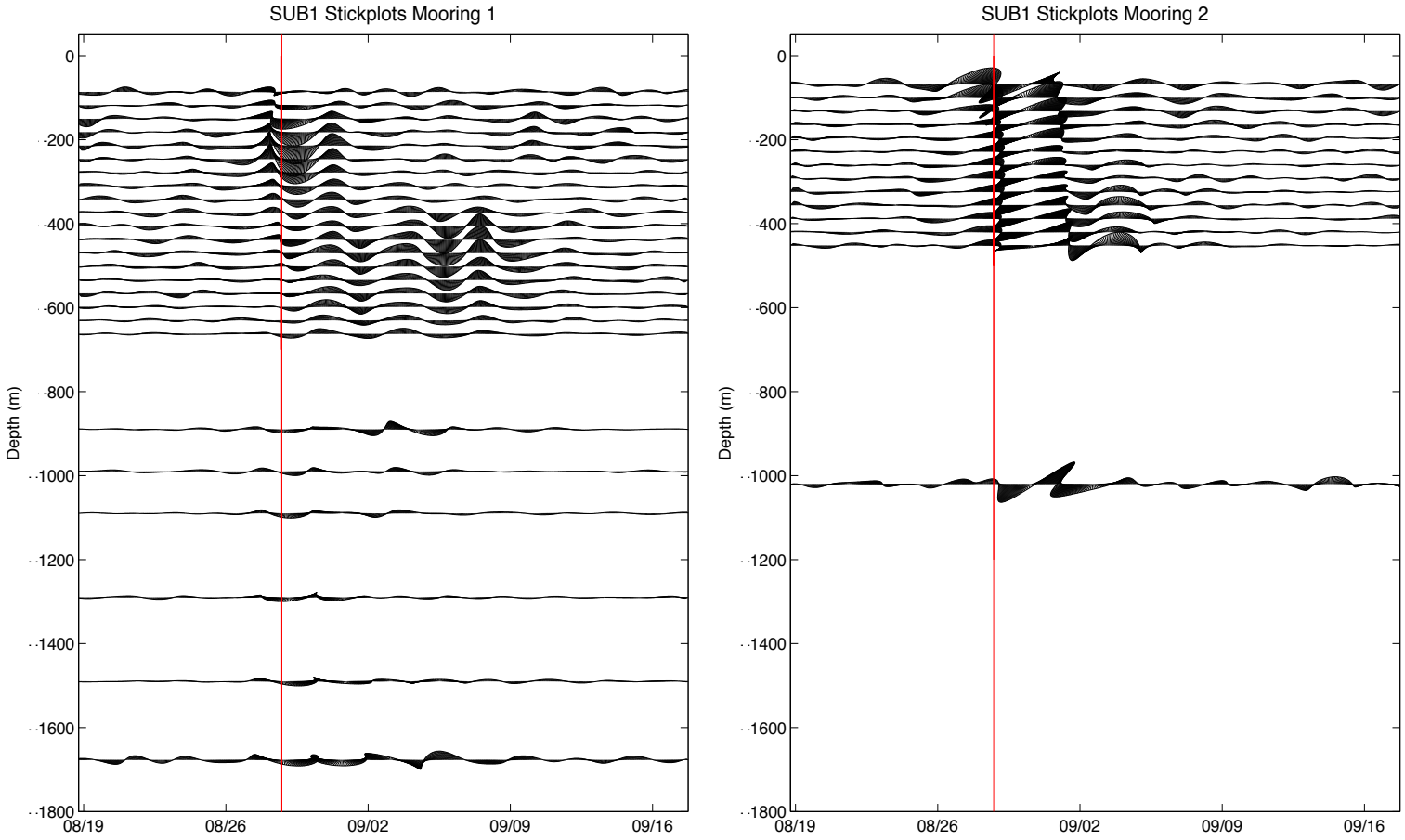


Figure 24. 2-5 Day Band Velocity Vector Plots. Velocity vector plots for 2-5 day period current meter data at each mooring 10 days before and 20 days after the passage of Hurricane Isaac are shown. The vertical red line represents the closest approach of Hurricane Isaac on August 28, 2012 at 18:00 UTC. The direction of the vectors is oceanographic convention with currents pointing up on the page referring to currents coming from the south and flowing north.

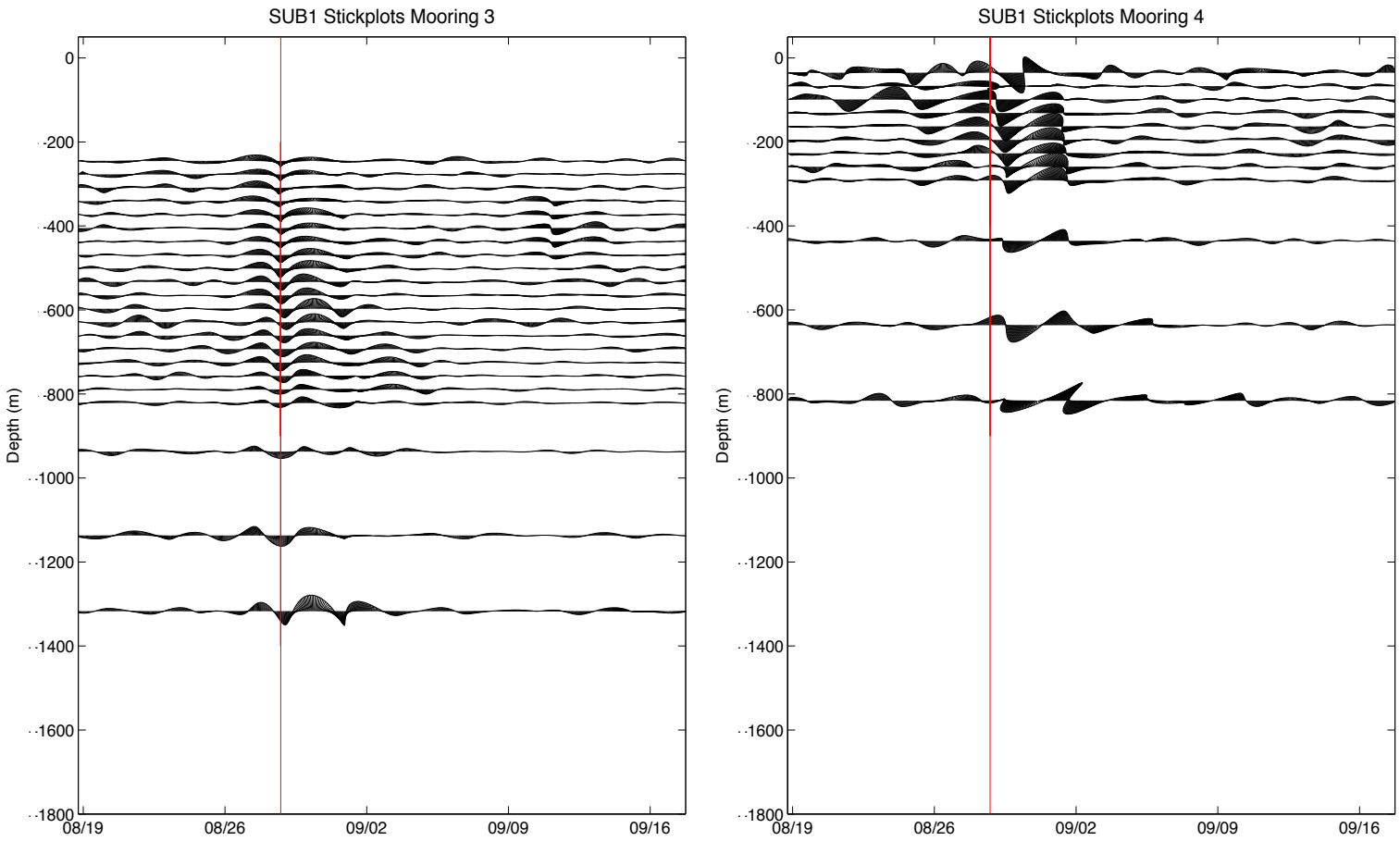


Figure 24 continued.

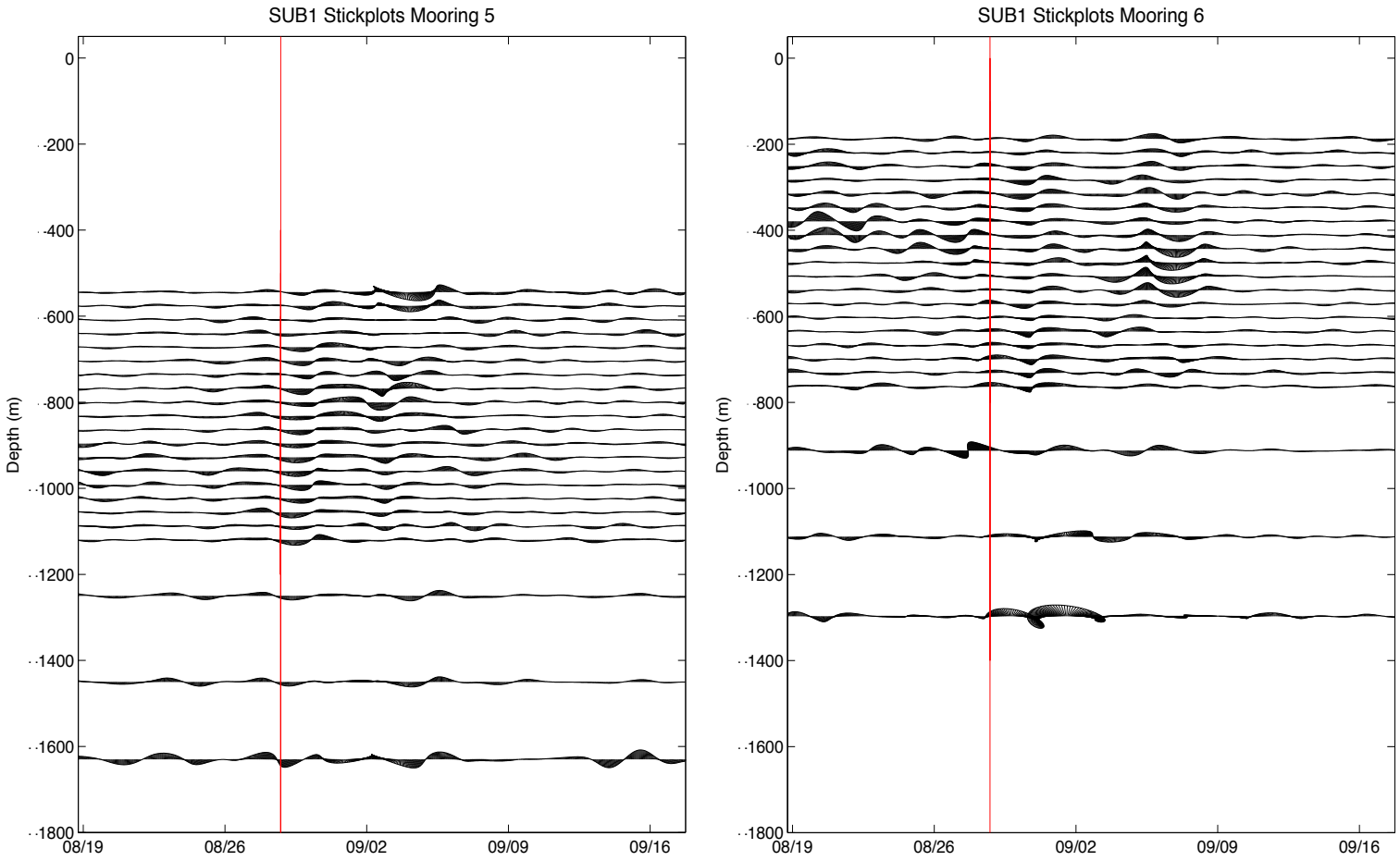


Figure 24 continued.

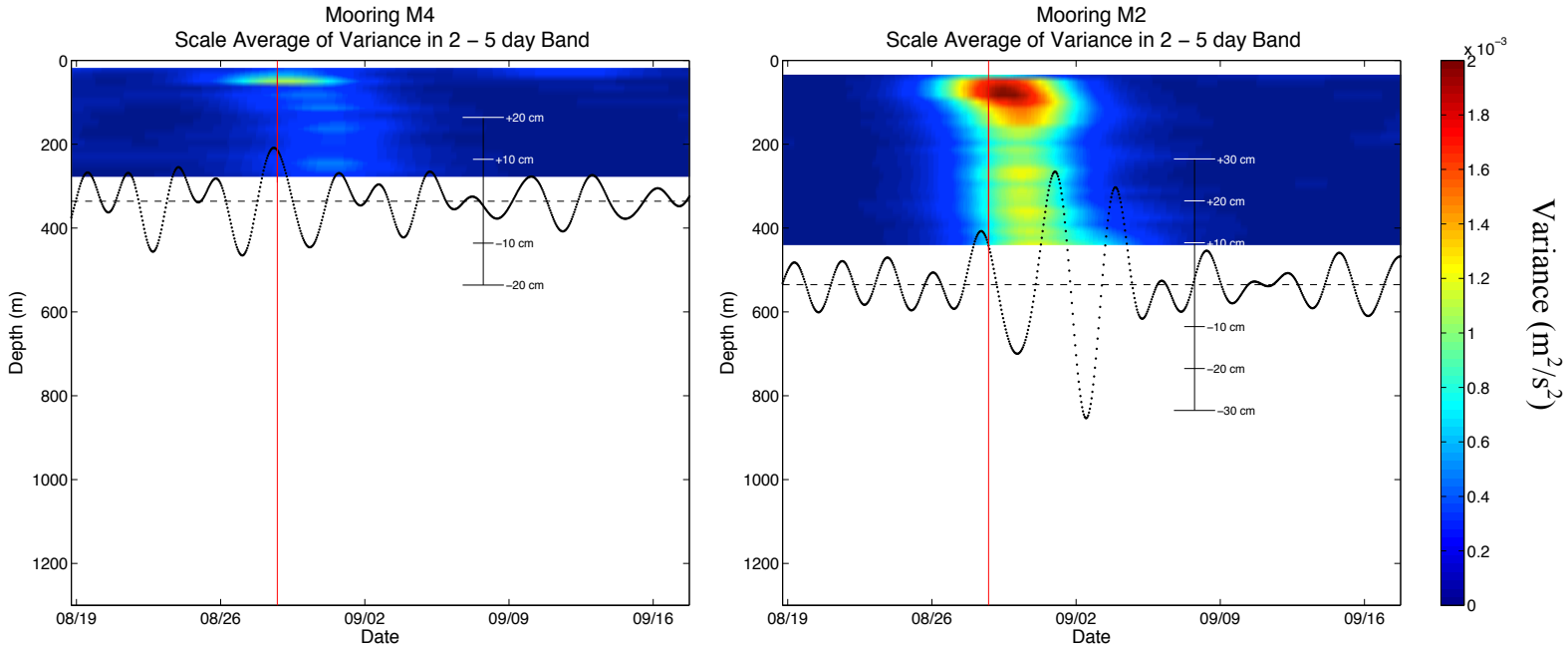


Figure 25. Scale Average of Variance in the 2-5 Day Band at Moorings 2 and 4. Scale average of variance for Mooring 2 and Mooring 4 in the SUB1 band from the east-west velocity component measured from the ADCP with overlay of the depth anomaly is shown. The red vertical line references the time of the closest approach of Hurricane Isaac to the mooring array on September 28, 2012 at 18:00 UTC. The depth anomaly derived from pressure data is shown as black dots in each figure. The black dashed line shows the deployment depth of the ADCP instrument.

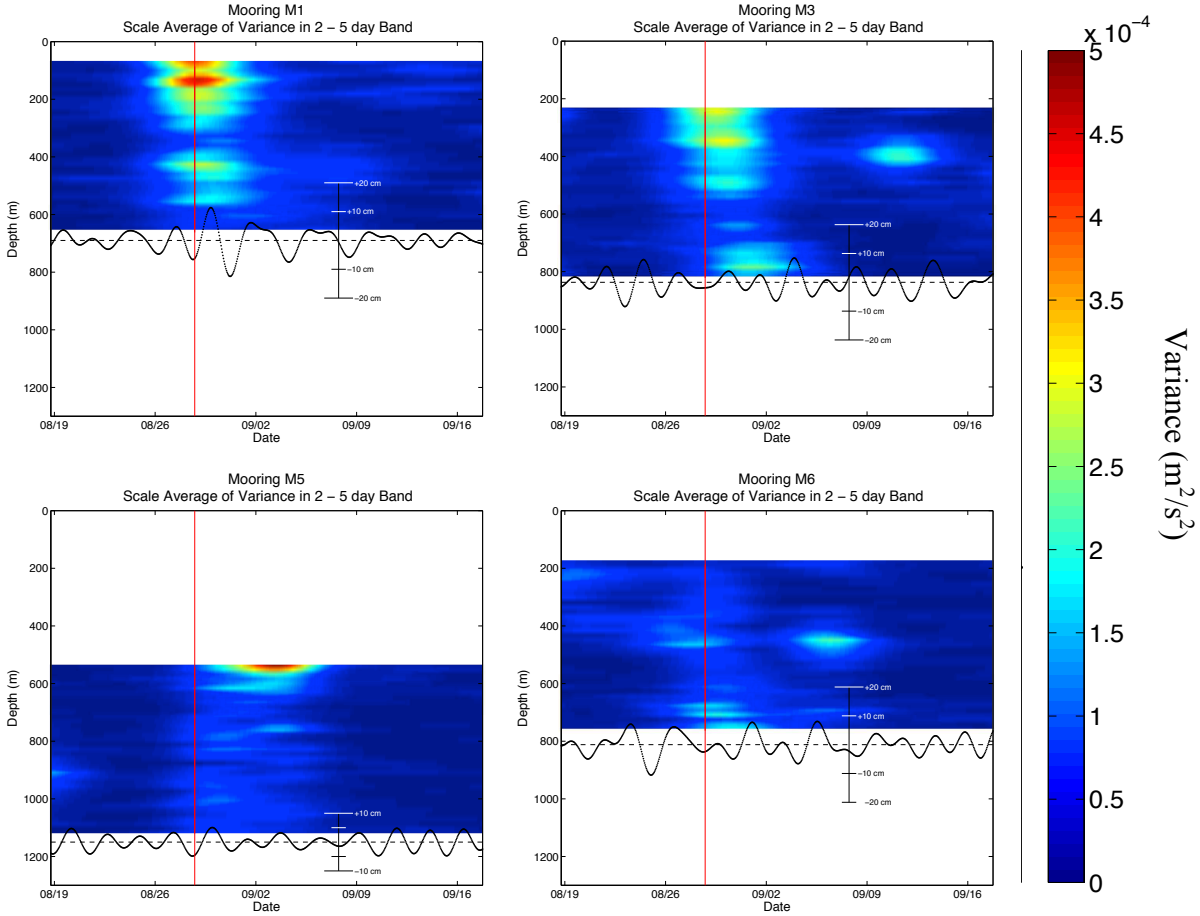


Figure 26. Scale Average of Variance in the 2-5 Day Band at Moorings 1, 3, 5, and 6. Scale average of variance in the SUB1 band from the east-west velocity component measured from the ADCP with overlay of the depth anomaly. The red vertical line references the time of the closest approach of Hurricane Isaac to the mooring array on September 28, 2012 at 18:00 UTC. The depth anomaly derived from pressure data is shown as black dots in each figure. The black dashed line shows the deployment depth of the ADCP instrument. Notice that the variance scale is different from Figure 25.

3.3.2.2 SUB2

The sub inertial band with a period between 5 and 12 days, SUB2, featured a relatively large percentage of the total variance in the current meter records associated with Hurricane Isaac. See Table 3for comparison of total variance explained by each band. Increases in speed and variance in this band are observed intermittently throughout the current meter records, but there is a consistent increase in speed observed during and after the passage of Hurricane Isaac at most of the mooring sites. Figure 27 shows that Moorings 2 and 4 observed the strongest speeds in this band with Mooring 4 experiencing maximum speeds of 11.1 cm/s near 200 m and Mooring 2 experiencing maximum speeds near 11.5 cm/s above 100 m. At Mooring 2, all observations of speeds greater than 10 cm/s were found in water depths less than 100 m. In contrast, maximum speeds at Mooring 4 were observed at depths of 300 m, which is the deepest the ADCP measured. Mooring 1 also observed a full water-column north and south surging pattern in the velocity records as shown in Figure 27, yet maximum speeds recorded were less than 9 cm/s. As with the SUB1 band, the response to Hurricane Isaac in the SUB2 band began before the arrival of the storm and persisted for approximately 7-10 days after the passage of the storm. The SUB2 band also observed a strong barotropic response, but some moorings (M1 and M3 in particular) experienced a reversal of coherence between 300 and 500 m indicative of a first mode response. The SUB2 band response is bottom intensified only at Moorings 2 and 5, while surface intensification is observed at Moorings 1, 2, 3, and 4. This response in the 5-12 day band is also indicative of a strong barotropic response to Hurricane Isaac just as in the 2-5 day sub-inertial band.

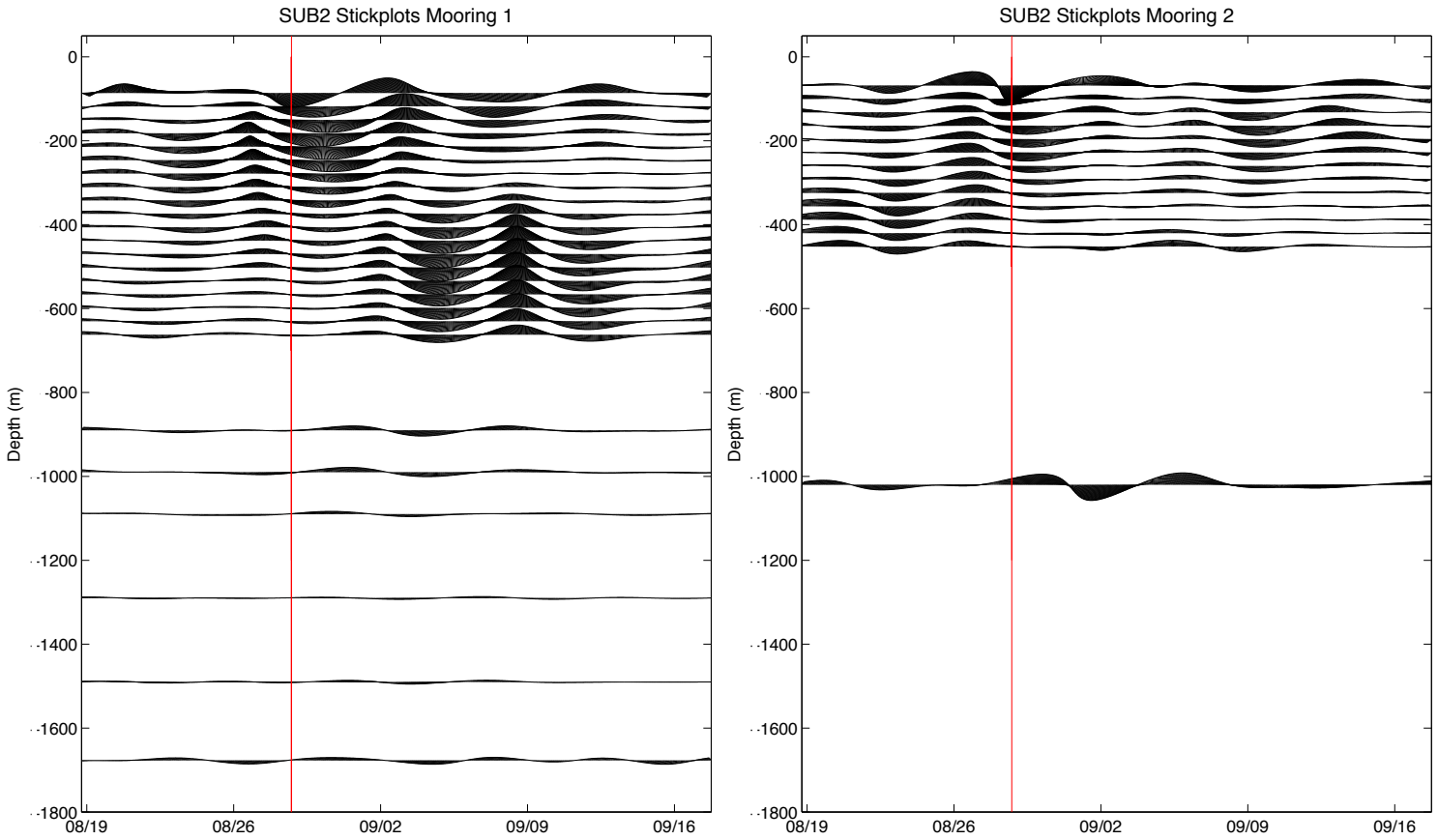


Figure 27. 5-12 Day Band Velocity Vector Plots. Velocity vector plots for 5-12 day period current meter data at each mooring 10 days before and 20 days after the passage of Hurricane Isaac are shown. The vertical red line represents the closest approach of Hurricane Isaac on August 28, 2012 at 18:00 UTC. The direction of the vectors is oceanographic convention with currents pointing up on the page referring to currents coming from the south and flowing north.

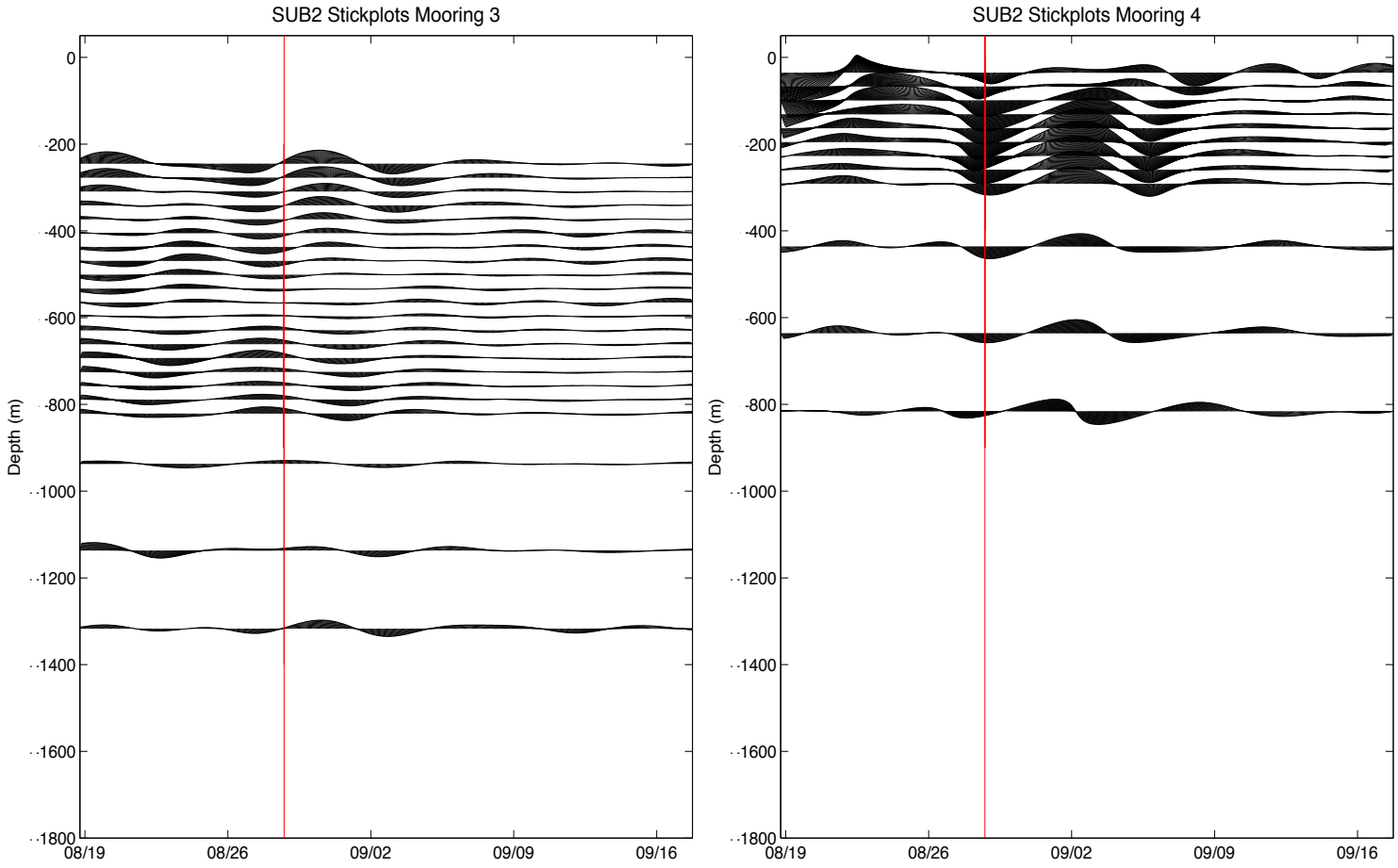


Figure 27 continued.

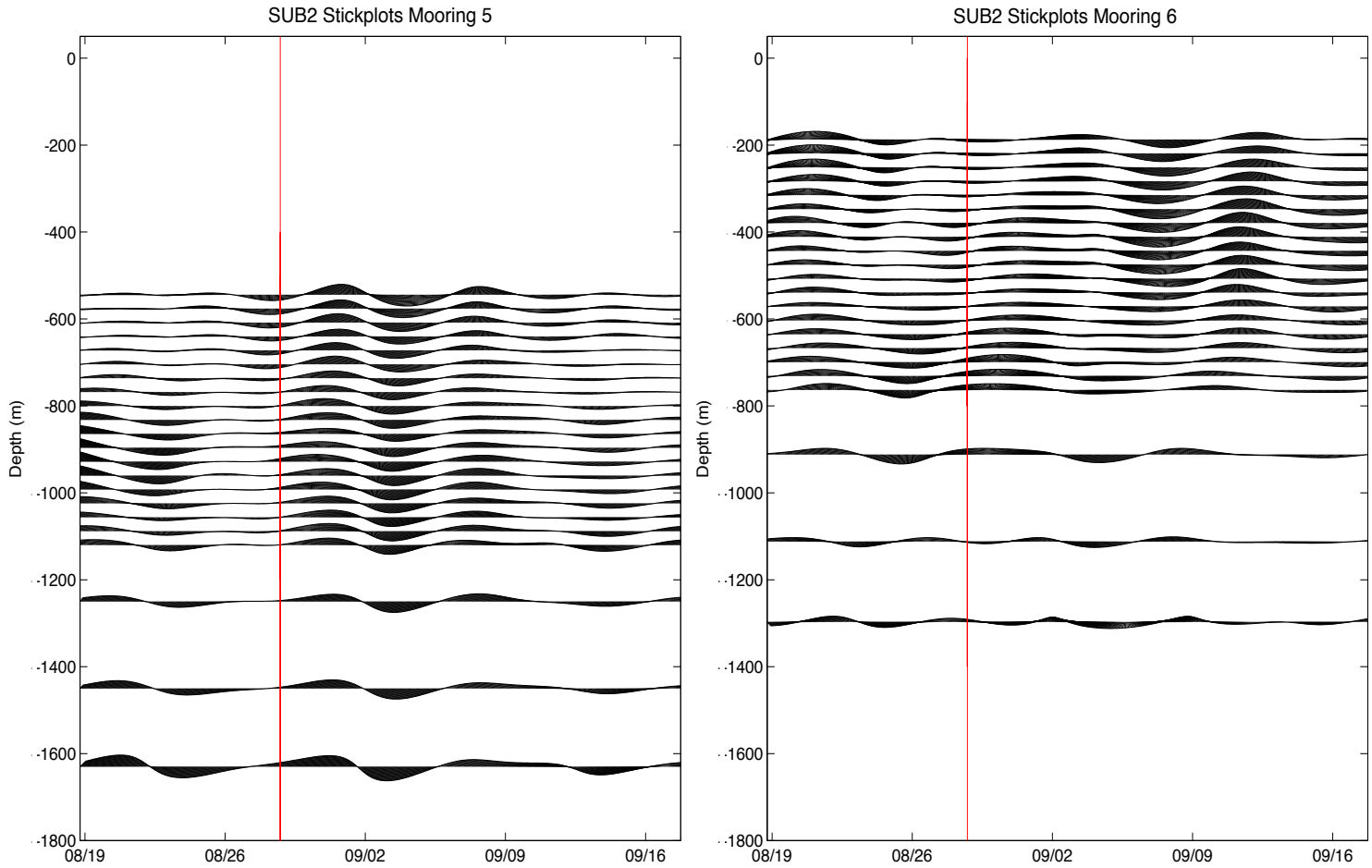


Figure 27 continued.

A strong barotropic response is observed in every mooring ADCP record in the 5-12 day sub-inertial band. As seen in the SUB1 band, Mooring 2 and Mooring 4 experienced a greater response in the SUB2 band associated with Hurricane Isaac. Figure 28 and Figure 29 show the wavelet products for the SUB2 response observed in each of the ADCP records. Figure 28 shows the shallower moorings, Mooring 2 and Mooring 4 on the same color scale. The amount of variance in the SUB2 bands of each mooring was less than the amount of variance found in the SUB1 band of each mooring. Mooring 2 experienced the largest amount of variance in the near surface region of the water column associated with the SUB2 band. The response observed in the SUB2 band also indicates a barotropic response. Although there is an increase in variance during the passage of Hurricane Isaac and in the storm's wake, energy in the SUB2 band is observed intermittently through the entire record.

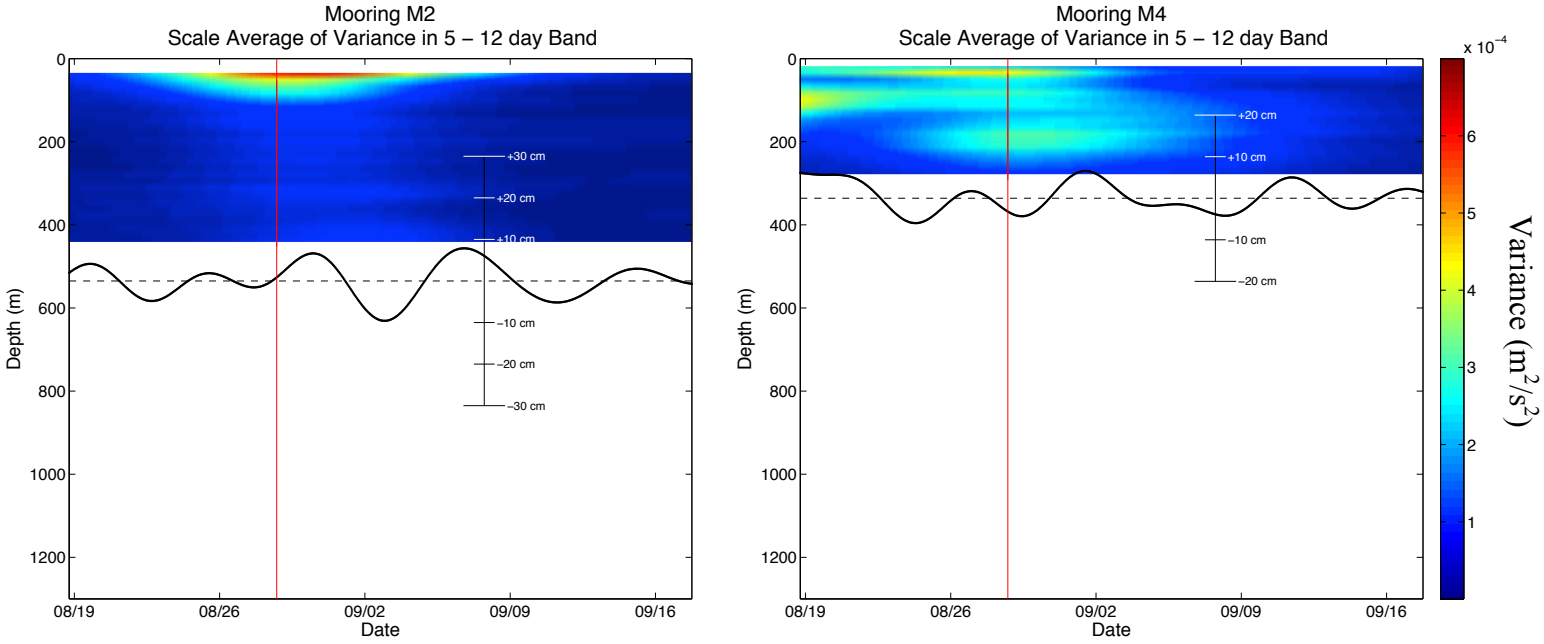


Figure 28. Scale Average of Variance in the 5-12 Day Band at Moorings 2 and 4. Scale average of variance for Mooring 2 and Mooring 4 in the SUB2 band from the east-west velocity component measured from the ADCP with overlay of the depth anomaly. The red vertical line references the time of the closest approach of Hurricane Isaac to the mooring array on September 28, 2012 at 18:00 UTC. The depth anomaly derived from pressure data is shown as black dots in each figure. The black dashed line shows the deployment depth of the ADCP instrument.

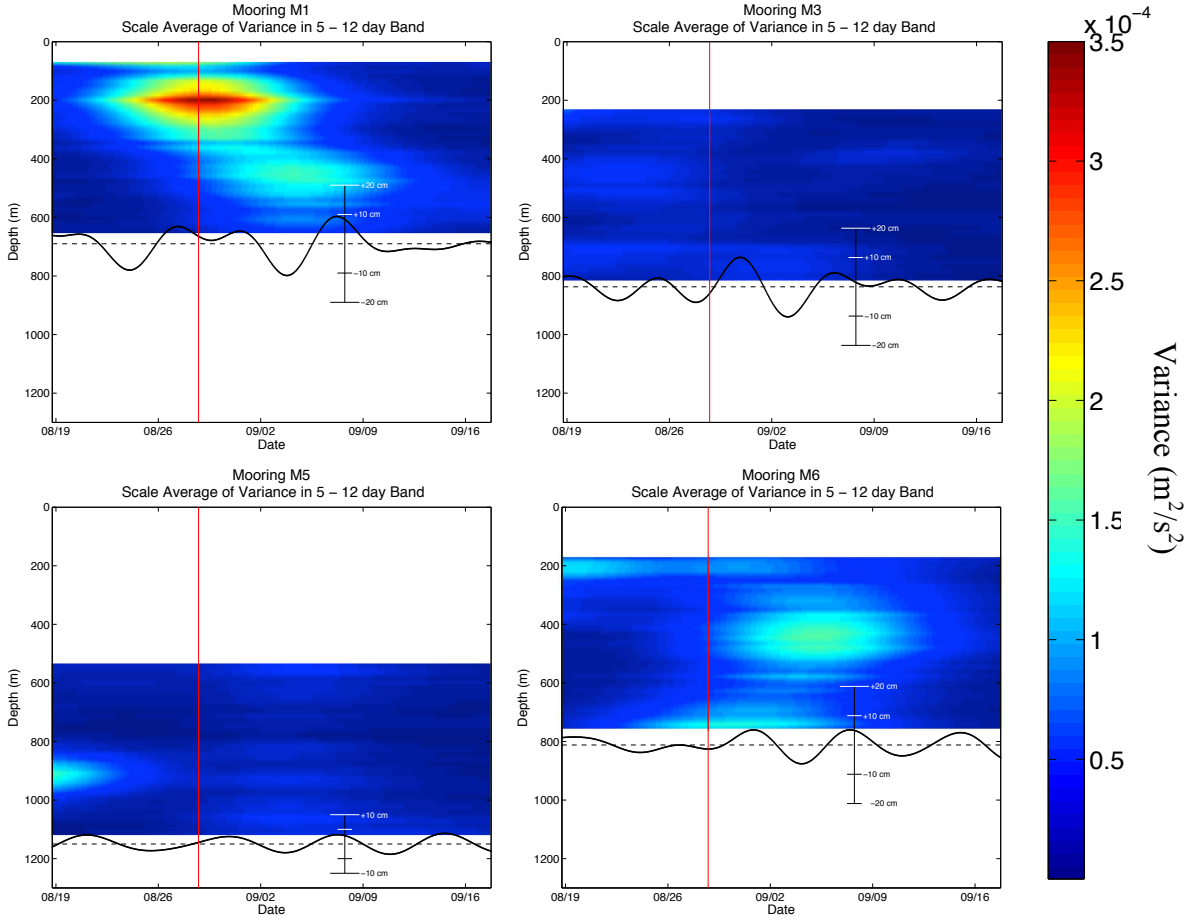


Figure 29. Scale Average of Variance in the 5-12 Day Band at Moorings 1, 3, 5, and 6. Scale average of variance in the SUB2 band from the east-west velocity component measured from the ADCP with overlay of the depth anomaly. The red vertical line references the time of the closest approach of Hurricane Isaac to the mooring array on September 28, 2012 at 18:00 UTC. The depth anomaly derived from pressure data is shown as black dots in each figure. The black dashed line shows the deployment depth of the ADCP instrument.

# 4. DISCUSSION

## 4.1 Hurricane Isaac

The characterization and description of the full water column near-inertial and sub-inertial response to Hurricane Isaac is presented in this study. Parameters to describe Hurricane Isaac were derived and compared to other storms in the Gulf of Mexico and the Northern Hemisphere and presented in Table 2. Hurricane Isaac, a Category 1 storm, was the least intense storm listed in the comparison. The translation speed of Hurricane Isaac (3.83 m/s) was only faster than Hurricane Norbert's translation speed of 3.0 m/s when it struck the Baja California Peninsula in 1984. The non-dimensional storm speed of Hurricane Isaac (.47) was considerably less than the compared hurricanes, which ranged between 1.0 and 2.4. In addition to the slower speeds, Hurricane Isaac also has a significantly larger radius of maximum winds, or cross track scale of 96 km compared to the other hurricanes which ranged from 20 km to 60 km. The estimated wind stress of Hurricane Isaac was only 1.35 $N/m^2$ compared with the other reported wind stress values between 4.0 and 6.7 $N/m^2$. The wind stress value for Hurricane Isaac was estimated from the product of a wind model in the Gulf of Mexico and not directly measured from flight data as in the case of the other hurricanes presented. This estimation from model output could be a reason for the lower wind stress value of Hurricane Isaac compared to the other hurricanes.

The Burger number, B, is a measure of the pressure coupling between the mixed layer current and the thermocline current. For Hurricane Isaac, B = .009 compared to the

other storms which ranges between .006 and .37. The Burger Number equation shows that the oscillations would be faster for smaller $R_{max}$ or weaker stratification. The $R_{max}$ for Hurricane Isaac was large compared to other storms, which is consistent with the Burger Number for Isaac being an order of magnitude less than other storms in the Gulf of Mexico.

The maximum measured currents associated with Hurricane Isaac showed maximum current speeds were found near the surface and in the wake of the storm. Despite the intense event of the storm's passage, the maximum currents observed in the current meter records were not associated with the passing of Hurricane Isaac. This implies that more energetic and persistent events, such as an eddy, impacted the mooring area, resulting in the maximum currents speeds observed throughout most of the water column.

**4.2 Oceanic Response**

Most notably, the near-inertial and sub-inertial responses observed in the wake of Hurricane Isaac showed a difference between the left and right sides of the storm path. The maximum currents were greater on the right side of the storm path compared to the left side. This is consistent with previous studies that observed sea surface temperature differences on each side of the storm track that lead to the expectation of a rightward bias of the storm's current response (Church, Joyce, and Price 1989, Sanford et al. 1987, Shay et al. 1998) (Shay et al. 1992). More energetic near-inertial motions were present on the right side of the storm track as also observed in the study of Hurricane Ivan (Teague et al. 2007). The left and right sides of the storm path also observed differences

in the response of relative vorticity to the passage of the storm. The passage of Hurricane Isaac, a strong cyclonic force, added positive relative vorticity to the mooring region as shown in Figure 16, but the increase in relative vorticity was not uniform on each side of the storm track. The right side of the storm path experienced a larger increase in relative vorticity compared to the left side. The wind stress values estimated for each side of the storm path also indicates a stronger response on the right side of the storm path compared to the left (Figure 18). Numerical ocean models have been used to explain that the directions of the wind stress vectors are responsible for the pronounced rightward bias of the response to a hurricane (Bender, Ginis, and Kurihara 1993, Price 1983).

In addition to the differences between currents observed on each side of the storm path, a noticeable difference was observed between the responses measured at the moorings deployed in shallower areas (less than 1050m) and moorings deployed in deeper water (between 1300 m and 1700 m), especially in the sub-inertial responses. The shallow mooring sites (Moorings 2 and 4) observed significantly larger amount of variance in the 2-5 day and 5-12 day sub-inertial responses after Hurricane Isaac as shown in Figure 25 and Figure 28. Less intense sub-inertial responses were observed at the deeper mooring sites. The more intense response at the shallower mooring sites could be explained by the influence of the continental shelf.

**4.3 Near-Inertial Response**

After the passage of Hurricane Isaac, a strong near-inertial response was observed in the current meter records. A large increase in variance in the near-inertial band was observed at all moorings. Moorings 1, 2, and 4 all experienced the maximum

increases in variance in the upper part of the water column as expected. Moorings 3, 5, and 6 all experienced maximum increases in variance associated with the near inertial band much deeper in the water column (between 700 and 900 m). This may be due to the deeper deployment of the moorings as with M5, or to the increased distance away from the storm track. The near-inertial response began immediately after the passage of the storm and persisted for approximately 10-15 days. This is similar to other observations of the near-inertial response to a hurricane in the Gulf of Mexico as documented in (Brooks 1983, Shay and Elsberry 1987, Teague et al. 2007).

The near-inertial response to Hurricane Isaac included the propagation of near-inertial energy away from the storm track and down to the thermocline over time. Moorings 1, 3 and 4 showed vertical propagation into the thermocline over time after the passage of Hurricane Isaac at a rate of approximately 29 m/day. Horizontal propagation speeds of approximately 5.7 km/day were calculated from phase shifts in the velocity records between moorings at similar depths. These values are comparable to the horizontal and vertical energy transport velocities of 23 km/day and 60 m/day observed in the wake of Hurricane Allen (Brooks 1983). These estimated horizontal and vertical group velocities for the near-inertial response to Hurricane Isaac were calculated using the average vertical and horizontal length scales and the estimated Brunt–Väisälä frequency. The vertical and horizontal scales of Hurricane Isaac were estimated to be .96 km and 205 km respectively. These scales are comparable to the vertical scale of ~1 km and the horizontal scale of 370 km determined for Hurricane Allen (Brooks 1983). Compared to Hurricane Allen, Hurricane Isaac was a much wider hurricane with an $R_{max}$

of 92.6 km to Allen's 20-40 km $R_{max}$. Hurricane Allen and Hurricane Isaac had similar translation speeds when crossing over mooring arrays, 3.83 m/s for Isaac and 3.5 m/s for Allen.

While Moorings 1, 3, and 4 showed propagation of energy into the thermocline over time, the near-inertial energy at Mooring 2 remained in the near-surface layer of the water column above 100 m. The inability for the near-inertial energy to penetrate into the thermocline may be explained by the background relative vorticity in the area near Mooring 2. Near inertial waves were shown to be stalled in the upper water column in areas of cyclonic circulation due to strengthened vertical shears and entrainment cooling (Jaimes and Shay 2010). Satellite altimetry figures show a transition region between cyclonic and anti-cyclonic rotation near Mooring 2 during the passage of Hurricane Isaac. Mooring 2 could have been subjected to a strong cyclonic relative vorticity that the course satellite altimetry products were not able to resolve.

After the passage of Hurricane Isaac, the amplitudes of the near-inertial waves increased then experienced an amplitude minimum before increasing again. Between 4 and 5 inertial periods after the storm, both Mooring 1 and Mooring 4 experience an amplitude minimum in the depths between 100 and 200 m. This type of amplitude minimum was also observed in the analysis of Hurricane Ivan (Teague et al. 2007) and was explained as possibly being related to a separation of the first baroclinic mode from other modes as suggested by the linear theory of Gill (1984).

### 4.3.1 Frequency Shift

The near-inertial frequency was also shifted above the local Coriolis frequency to 1.11$f$ in the wake of Hurricane Isaac. A similar blue shift in near-inertial frequency in response to a hurricane was observed by Shay et al. (1998) in the study of Hurricane Gilbert in 1988 and by Jaimes and Shay (2010) in the study of Hurricanes Katrina and Rita in 2005. Teague et al. (2007), Shay and Elsberry (1987), and Schuster (2013) also found similar shifts in frequency after Hurricane Ivan in 2004 and Hurricane Frederic in 1979. The observed blue shift in frequency in the near-inertial band suggests a strong influence of the background vorticity field on the near-inertial response. It has been shown that the effective frequency of the near-inertial motion can be shifted above the local Coriolis frequency by the relative vorticity of the mean flow as $f_{\text{eff}} = f + \zeta/2$ (Mooers 1975, Kunze 1985).

The relative vorticity for the study region was calculated around the time of Hurricane Isaac and compared with satellite altimetry products. The relative vorticity was calculated from the available current meter records at similar depths. The satellite altimetry figures did not fully align with the observed currents and calculated relative vorticity for the study region. This is due in part to the course resolution of the altimetry product combined with smoothing applied to the satellite data. The altimetry products show a transitional region between sea surface heights being above and below the mean sea level near the northeastern region of the mooring array. This transitional region could explain some of the discrepancies found between the relative vorticity estimates

derived from the current meter records and the expected current directions implied from the satellite altimetry products.

### 4.4 Sub-Inertial Response

The observed sub-inertial response to Hurricane Isaac was fundamentally different than the near-inertial response. The near-inertial response was strongly barotropic and observed through the entire water column immediately after the passage of the storm. Wavelet analysis showed two distinct sub-inertial responses, one with a period of 2-5 days and another with a period of 5-12 days. The propagation direction and scales of these waves were unable to be determined from the current meter data available in this study. No clear propagation direction could be determined implying that these sub-inertial wave were non-propagating which is consistent with a barotropic response. Analysis of sea level height derived from pressure data collected on each ADCP indicated that changes in sea level height associated with each band during the time of Hurricane Isaac's passage aligned with increased in variability in each band. This is also suggestive of a barotropic response, but this work has not gone far enough to prove this.

Other studies observed similar sub-inertial responses to hurricanes. A sub-inertial wave with a period between 2 and 5 days was observed in response to Hurricane Ivan in 2004 (Teague et al. 2007). This study concluded that the sub-inertial wave could be a topographic Rossby wave based on the propagation direction, bottom intensification and highly correlated and nearly in phase currents below 150 m. A sub-inertial wave with a period between 2 and 10 days was observed in the post-storm relaxation stage of tropical Cyclone Gonu in the northern Arabian Sea in 2007 (Wang et al. 2012). Another

prominent sub-inertial wave with a period of 12.7 days was also measured after tropical Cyclone Gonu. This 12.7 day sub-inertial wave had characteristics of baroclinic topographically trapped wave. The sub-inertial response did show highly correlated and nearly in phase currents throughout the water column, and a slight bottom intensification was observed in the current meter data from some moorings, but the propagation direction was unable to be determined for either sub-inertial wave. The sub-inertial responses to Hurricane Ivan were likely not a topographic Rossby wave, but instead just a strong barotropic response.

# 5. CONCLUSION

In late July 2012, six deepwater mooring were deployed in the Mississippi Fan region of the Gulf of Mexico as part of the Gulf Integrated Spill Research Project. Each mooring featured an upward-looking 75 kHz Acoustic Doppler Current Profiler as well as other current meters and oceanographic instrumentation deployed throughout the water column. The moorings were recovered the following summer and all moorings except Mooring 2 were fully recovered. Mooring 2 experienced complications with recovered that resulted in the loss of the lower water column instruments. CTD casts were taken on both the mooring deployment cruise in July 2012 and on the recovery cruise in July 2013 to determine the hydrography for the mooring region.

In late August 2012, Tropical Storm Isaac entered the Gulf of Mexico through the Florida Straits before increasing in strength to a Category 1 hurricane. On August 28, 2012 Hurricane Isaac approached the GISR mooring array and passed directly over the moorings with Moorings 1, 2, and 3 on the right side of the storm path, and Moorings 4, 5, and 6 on the left side of the storm path. Data from the CTD casts along with reported feature of the hurricane and output form a wind model were used to calculate the parameters for Hurricane Isaac. Hurricane Isaac was a relatively wide and slow moving storm compared to previously studied hurricanes in the Gulf of Mexico. The current response to Hurricane Isaac was observed by all mooring instrumentation deployed throughout the water column, with a 16 m vertical resolution captured by the ADCP deployed at the top of each mooring.

The current meter data from each ADCP as well as each RCM and S4A current meter were quality controlled, subsampled to an hourly grid and detided. Wavelet analysis was used to identify periods of high variability in response to Hurricane Isaac and indicated a strong near-inertial response in the upper water column and two sub-inertial responses throughout the water column. The records were then band passed into a near-inertial band, near 1-day period, and two sub-inertial bands, one with a 2-5 day period and another with a 5-12 day period.

Relative vorticity was estimated for each side of the hurricane track from available current meter records at similar depths. A strong negative vorticity was observed on the right side of the storm track before the arrival of Hurricane Isaac indicating anticyclonic circulation. The left side of the storm track experienced positive relative vorticity indicating cyclonic circulation. The relative vorticity on each side of the storm track increased with the passage of the strong cyclonic hurricane. The right side of the storm path experienced the strongest increase relative vorticity after the passage of the storm compared to the left side of the storm. Maximum currents observed in response to Hurricane Isaac also showed stronger currents on the right side of the storm track compared to the left side. This rightward bias was also observed in the wind stress analysis.

The analysis of the near-inertial band showed a strong increase in variability in the upper water column and a slight increase in phase with depth. This depth-leading phase is indicative of downward propagation of energy into the thermocline. Near-inertial energy was observe propagating away from the storm track at rate of

approximately 5.7 km/day and down into the thermocline at a rate of approximately 29 m/day. The near-inertial response was stronger at moorings deployed of the right side of the storm path compared to the left side of the storm path. A shift in the near-inertial frequency above the local Coriolis frequency was observed after 1-2 inertial periods following the passage of the storm and persisted for almost 5 inertial periods. This blue shift of 1.11$f$ was observed in the ADCP current records from each mooring and the background relative vorticity was thought to be the cause of this frequency shift.

In addition to the strong near-inertial response, a fundamentally different sub-inertial response was observed throughout the water column in response to Hurricane Isaac. The sub-inertial response consisted of two separate responses with periods between 2-5 days and 5-12 days. The 2-5 day sub-inertial response began approximately 1-2 inertial periods before the closest approach of the hurricane and persisted for 5-7 days. The 5-12 day sub-inertial band also began approximately 1-2 inertial periods before the closest approach of the storm but persisted for 7-10 days. The sub-inertial responses were vertically coherent and barotropic. The horizontal and vertical propagation speeds and directions were unable to be determined due to no clear and consistent phase shifts observed between moorings at similar depths.

The shallower moorings, Mooring 2 and Mooring 4, experienced the strongest response in both sub-inertial bands in response to Hurricane Isaac. The 2-5 day sub-inertial band experienced both surface and bottom intensification at most moorings, but the 5-12 day sub-inertial band experienced a slight surface intensification and little to no bottom intensification. The moorings deployed in deeper water observed an increase in

variability, but not to the same degree as the shallower moorings. This difference between the sub-inertial response at shallower and deeper regions may be due to the interaction of energy with the topography and continental shelf.

The take away points from this study should be that in response to Hurricane Isaac, a strong near-inertial and sub-inertial response was observed in the mooring data. A clear difference was observed in the near-inertial response between the left and right side of the storm path, with increases in speeds and variance on the right side. In the sub-inertial responses, a clear difference was observed between the data collected from moorings deployed in shallower regions compared to moorings deployed in deeper regions. These findings will be useful for the continued validation and improvement of numerical ocean circulation models for this region of the Gulf of Mexico. This description of the full water column oceanic response to Hurricane Isaac along with the calculated hurricane parameters will be used to improve the model's capabilities to capture near-inertial and sub-inertial responses from future extreme events in the Gulf of Mexico.

WORKS CITED

Bender, L. C., and S. F. DiMarco. 2009. Quality Control Analysis of Acoustic Doppler Current Profiler Data Collected on Offshore Platforms of the Gulf of Mexico. Texas A&M University., College Station.

Bender, M. A., I. Ginis, and Y. Kurihara. 1993. "Numerical Simulations of Tropical Cyclone-Ocean Interaction with a High-Resolution Coupled Model." *Journal of Geophysical Research-Atmospheres* 98 (D12):23245-23263. doi: 10.1029/93jd02370.

Berg, R. J. 2013. "Tropical Cyclone Report Hurricane Isaac." Accessed 10-16-2013. http://www.nhc.noaa.gov/data/tcr/AL092012_Isaac.pdf.

Bloomfield, P. 1976. *Fourier Analysis of Time Series: An Introduction*: Wiley.

Brooks, D. A. 1983. "The Wake of Hurricane Allen in the Western Gulf of Mexico." *Journal of Physical Oceanography* 13 (1):117-129. doi:10.1175/1520-0485(1983)013<0117:Twohai>2.0.Co;2.

Church, J. A., T. M. Joyce, and J. F. Price. 1989. "Current and Density Observations across the Wake of Hurricane Gay." *Journal of Physical Oceanography* 19 (2):259-265. doi: 10.1175/1520-0485(1989)019<0259:Cadoat>2.0.Co;2.

DiMarco, S. F., and R. O. Reid. 1998. "Characterization of the Principal Tidal Current Constituents on the Texas-Louisiana Shelf." *Journal of Geophysical Research-Oceans* 103 (C2):3093-3109. doi: 10.1029/97jc03289.

Duchon, C. E. 1979. "Lanczos Filtering in One and 2 Dimensions." *Journal of Applied Meteorology* 18 (8):1016-1022. doi: 10.1175/1520-0450(1979)018<1016:Lfioat>2.0.Co;2.

Emery, William J., and Richard E. Thomson. 2001. *Data Analysis Methods in Physical Oceanography*. Edited by Richard E. Thomson. Amsterdam Elsevier.

Gill, A. E. 1984. "On the Behavior of Internal Waves in the Wakes of Storms." *Journal of Physical Oceanography* 14 (7):1129-1151. doi: 10.1175/1520-0485(1984)014<1129:Otboiw>2.0.Co;2.

Grinsted, A., J. C. Moore, and S. Jevrejeva. 2004. "Application of the Cross Wavelet Transform and Wavelet Coherence to Geophysical Time Series." *Nonlinear Processes in Geophysics* 11 (5-6):561-566.

Hamilton, P. 1990. "Deep Currents in the Gulf of Mexico." *Journal of Physical Oceanography* 20 (7):1087-1104. doi:10.1175/1520-0485(1990)020<1087:Dcitgo>2.0.Co;2.

Jaimes, B., and L. K. Shay. 2009. "Mixed Layer Cooling in Mesoscale Oceanic Eddies during Hurricanes Katrina and Rita." *Monthly Weather Review* 137 (12):4188-4207. doi:10.1175/2009mwr2849.1.

Jaimes, B., and L. K. Shay. 2010. "Near-Inertial Wave Wake of Hurricanes Katrina and Rita over Mesoscale Oceanic Eddies." *Journal of Physical Oceanography* 40 (6):1320-1337. doi: 10.1175/2010jpo4309.1.

Kunze, E. 1985. "Near-Inertial Wave-Propagation in Geostrophic Shear." *Journal of Physical Oceanography* 15 (5):544-565. doi:10.1175/1520-0485(1985)015<0544:Niwpig>2.0.Co;2.

Large, W. G., and S. Pond. 1981. "Open Ocean Momentum Flux Measurements in Moderate to Strong Winds." *Journal of Physical Oceanography* 11 (3):324-336. doi:10.1175/1520-0485(1981)011<0324:Oomfmi>2.0.Co;2.

Liu, Y. G., X. S. Liang, and R. H. Weisberg. 2007. "Rectification of the Bias in the Wavelet Power Spectrum." *Journal of Atmospheric and Oceanic Technology* 24 (12):2093-2102. doi: 10.1175/2007jtecho511.1.

Mooers, C. N. K. 1975. "Several Effects of a Baroclinic Current on the Cross-Stream Propagation of Inertial-Internal Waves." *Geophysical fluid dynamics* 6 (3):245-275.

Muller, P., R. C. Lien, and R. Williams. 1988. "Estimates of Potential Vorticity at Small Scales in the Ocean." *Journal of Physical Oceanography* 18 (3):401-416. doi: 10.1175/1520-0485(1988)018<0401:Eopvas>2.0.Co;2.

Nelson, Craig S., and United States. National Marine Fisheries Service. 1977. *Wind Stress and Wind Stress Curl over the California Current*, *NOAA technical report NMFS SSRF-714*. Seattle, Washington: U.S. Dept. of Commerce, National Oceanic and Atmospheric Administration for sale by Supt. of Docs., U.S. Govt Print. Office.

Oey, L. Y. 2008. "Loop current and deep eddies." *Journal of Physical Oceanography* 38 (7):1426-1449. doi: 10.1175/2007jpo3818.1.

Price, J. F. 1983. "Internal Wave Wake of a Moving Storm .1. Scales, Energy Budget and Observations." *Journal of Physical Oceanography* 13 (6):949-965. doi: 10.1175/1520-0485(1983)013<0949:Iwwoam>2.0.Co;2.

Price, J. F., T. B. Sanford, and G. Z. Forristall. 1994. "Forced Stage Response to a Moving Hurricane." *Journal of Physical Oceanography* 24 (2):233-260. doi: 10.1175/1520-0485(1994)024<0233:Fsrtam>2.0.Co;2.

Qi, H. B., R. A. Deszoeke, C. A. Paulson, and C. C. Eriksen. 1995. "The Structure of near-Inertial Waves during Ocean Storms." *Journal of Physical Oceanography* 25 (11):2853-2871. doi:10.1175/1520-0485(1995)025<2853:Tsoniw>2.0.Co;2.

Sanford, T. B., P. G. Black, J. R. Haustein, J. W. Feeney, G. Z. Forristall, and J. F. Price. 1987. "Ocean Response to a Hurricane Part 1. Observations." *Journal of Physical Oceanography* 17 (11):2065-2083. doi:10.1175/1520-0485(1987)017<2065:Ortahp>2.0.Co;2.

Schuster, R. M. . 2013. "The Near-Inertial Response to Hurricane Ivan." Master of Science, Meteorology and Physical Oceanography, University of Miami (457).

Shay, L. K., P. G. Black, A. J. Mariano, J. D. Hawkins, and R. L. Elsberry. 1992. "Upper Ocean Response to Hurricane Gilbert." *Journal of Geophysical Research-Oceans* 97 (C12):20227-20248. doi: 10.1029/92jc01586.

Shay, L. K., and S. W. Chang. 1995. "Free Surface Effects on the Near-Inertial Ocean Current Response to a Hurricane: A rRevisit." *21st Conference on Hurricanes and Tropical Meteorology*:532-534.

Shay, L. K., and R. L. Elsberry. 1987. "Near-Inertial Ocean Current Response to Hurricane Frederic." *Journal of Physical Oceanography* 17 (8):1249-1269. doi: 10.1175/1520-0485(1987)017<1249:Niocrt>2.0.Co;2.

Shay, L. K., R. L. Elsberry, and P. G. Black. 1989. "Vertical Structure of the Ocean Current Response to a Hurricane." *Journal of Physical Oceanography* 19 (5):649-669. doi:10.1175/1520-0485(1989)019<0649:Vsotoc>2.0.Co;2.

Shay, L. K., A. J. Mariano, S. D. Jacob, and E. H. Ryan. 1998. "Mean and Near-Inertial Ocean Current Response to Hurricane Gilbert." *Journal of Physical Oceanography* 28 (5):858-889. doi:10.1175/1520-0485(1998)028<0858:Manioc>2.0.Co;2.

Stommel, Henry M. 1958. *The Gulf Stream: A Physical and Dynamical Description*. Berkeley: Berkeley, University of California Press.

Talley, L.D., G.L. Pickard, W.J. Emery, and J.H. Swift. 2011. *Descriptive Physical Oceanography: An Introduction*: Elsevier Science.

Teague, W. J., E. Jarosz, D. W. Wang, and D. A. Mitchell. 2007. "Observed Cceanic esponse Over the Upper Continental Slope and Outer Shelf During Hurricane Ivan." *Journal of Physical Oceanography* 37 (9):2181-2206. doi: 10.1175/Jpo3115.1.

Thompson, R. O. R. Y. 1979. "Coherence Significance Levels." *Journal of the Atmospheric Sciences* 36 (10):2020-2021. doi:10.1175/1520-0469(1979)036<2020:Csl>2.0.Co;2.

Torrence, C., and G. P. Compo. 1998. "A Practical Guide to Wavelet Analysis." *Bulletin of the American Meteorological Society* 79 (1):61-78. doi:10.1175/1520-0477(1998)079<0061:Apgtwa>2.0.Co;2.

Wang, Z. K., S. F. DiMarco, M. M. Stossel, X. Q. Zhang, M. K. Howard, and K. du Vall. 2012. "Oscillation Responses to Tropical Cyclone Gonu in Northern Arabian Sea from a Moored Observing System." *Deep-Sea Research Part I-Oceanographic Research Papers* 64:129-145. doi: 10.1016/J.Dsr.2012.02.005.

Welch, P. D. 1967. "Use of Fast Fourier Transform for Estimation of Power Spectra - a Method Based on Time Averaging over Short Modified Periodograms." *Ieee Transactions on Audio and Electroacoustics* Au15 (2):70-&. doi: 10.1109/Tau.1967.1161901.

Zheng, Q. N., R. J. Lai, N. E. Huang, J. Y. Pan, and L. W. Timothy. 2006. "Observation of Ocean Current Response to 1998 Hurricane Georges in the Gulf of Mexico." *Acta Oceanologica Sinica* 25 (1):1-14.